

Nonleptonic two-body weak decays of charmed baryons

Chia-Wei Liu *Tsung-Dao Lee Institute, Shanghai Jiao Tong University, Shanghai 200240, China* (Received 23 October 2023; accepted 8 January 2024; published 5 February 2024)

We analyze the two-body nonleptonic weak decays of charmed baryons, employing the pole approximation in tandem with the $SU(3)_F$ symmetry. We are able to make novel predictions for decay channels of $\Omega_c^0 \rightarrow \mathbf{B}_n P$ and $\mathbf{B}_{cc} \rightarrow \mathbf{B}_c^{A,S} P$ based on the experimental data of $\mathbf{B}_c^A \rightarrow \mathbf{B}_n P$. Here, \mathbf{B}_n , \mathbf{B}_c^A , \mathbf{B}_c^S , and \mathbf{B}_{cc} are the low-lying octet, antitriplet charmed, sextet charmed and doubly charmed baryons, respectively, and P is the pseudoscalar meson. Our findings reveal that the fitted effective Wilson coefficient $C_+ = 0.469$ is notably smaller than the naïve expectation, and the low-lying pole approximation fails to account for $\mathcal{B}(\Lambda_c^+ \rightarrow n\pi^+, \Xi^0 K^+)$, despite consistencies with the soft meson limit. We further recommend the decay channel $\Xi_{cc}^+ \rightarrow \Xi_c^0 \pi^+ \rightarrow \Xi^- \pi^+ \pi^+ \pi^+ \pi^-$ for exploring evidence of Ξ_{cc}^+ , estimating the branching fraction at $(1.1 \pm 0.6) \times 10^{-3}$.

DOI: [10.1103/PhysRevD.109.033004](https://doi.org/10.1103/PhysRevD.109.033004)

I. INTRODUCTION

The investigation into charmed baryon decays has attracted significant theoretical interest, driven further by the progress in experiments [1]. For a review, readers are referred to Refs. [2,3]. At the BESIII facility, the lightest charmed baryon, Λ_c^+ , has been rigorously examined through e^+e^- interactions at a central energy of $\sqrt{s} = 4.6$ GeV [4]. These investigations have yielded remarkably precise measurements of branching fractions and decay asymmetries [5–7]. The resonance structure of $e^+e^- \rightarrow \Lambda_c^+ \Lambda_c^-$, providing a clean background, has facilitated the BESIII Collaboration’s ability to measure $\Lambda_c \rightarrow n\pi^+$ in spite of the challenges posed by neutrons [8]. However, the comprehensive study of the entire charmed baryon family necessitates the synthesis of results from multiple experimental facilities, as only Λ_c^+ is currently accessible at BESIII.

Through the B meson decay chain, the Belle Collaboration has access to all the low-lying antitriplet charmed baryons ($\mathbf{B}_c^A = \Lambda_c^+, \Xi_c^+, \Xi_c^0$) [9–12]. A significant recent breakthrough includes the measurement of absolute branching fractions for $\Xi_c^0 \rightarrow \Xi^- \pi^+$ [13] and $\Xi_c^0 \rightarrow \Xi^- e^+ \nu_e$ [14], revealing substantial $SU(3)_F$ symmetry breaking [15]. Conversely, the LHCb Collaboration has obtained the largest charmed hadron samples from pp collisions at $\sqrt{s} = 7, 8, 12$ GeV. Despite more complex backgrounds compared to those at BESIII and Belle, the majority of new

charmed baryon discoveries [16], including the famed doubly charmed baryon [17], have been made at LHCb. Additionally, Belle and LHCb have revisited the lifetimes of certain baryons [18,19], with notable deviations found in the measured lifetimes of Ξ_c^0 and Ω_c^0 compared to previous experiments [20]. These measurements, however, are consistent with the heavy quark expansion (HQE) [21–23].

Thanks to the optical theorem, the inclusive decay widths of charmed hadrons can be at least qualitatively studied [24]. It is understood that the contributions of the dimension-6 operators in the HQE, suppressed by $(\Lambda_{\text{QCD}}/M_c)^3$, may exceed those of the dimension-3 operators due to phase space enhancement [25]. This emphasizes the leading role of the W -exchange diagrams in decays. However, as of now, there is no reliable method derived from first principles to address the W -exchange diagrams in exclusive decays, leading to the need for several approximations [26–40]. One less model-dependent approach is to perform a global fit using the $SU(3)$ flavor [$SU(3)_F$] symmetry, which has become popular [41–61]. Nevertheless, even in the simplest case of $\mathbf{B}_c^A \rightarrow \mathbf{B}_n P$, where \mathbf{B}_n and P represent the octet baryon and pseudoscalar meson respectively, this method requires dozen one-time parameters. While the results of the global fit often align with the experimental data used for fitting, the predictive accuracy is disputable. The predicted branching fractions significantly diverge across various theoretical studies relying on the $SU(3)_F$ symmetry, illustrating that the free parameters are not tightly constrained by the existing experimental data.

In an effort to reduce the number of free parameters in the $SU(3)_F$ global fit, Geng, Tsai, and the author of this work considered the pole approximation in 2019 [49,50].

Published by the American Physical Society under the terms of the Creative Commons Attribution 4.0 International license. Further distribution of this work must maintain attribution to the author(s) and the published article’s title, journal citation, and DOI. Funded by SCOAP³.

This approach, grounded in the Körner-Pati-Woo (KPW) theorem [62], enables the exclusion of six parameters from $O_+^{qq'}$. Here $O_+^{qq'}$ is the four-quark operator in the effective Hamiltonian [63]

$$\mathcal{H}_{\text{eff}} = \sum_{q,q'=d,s} \frac{G_F}{\sqrt{2}} V_{cq}^* V_{uq'} (c_+ O_+^{qq'} + c_- O_-^{qq'}), \quad (1)$$

with

$$O_{\pm}^{qq'} = \frac{1}{2} [(\bar{u}q')_{V-A}(\bar{q}c)_{V-A} \pm (\bar{q}q')_{V-A}(\bar{u}c)_{V-A}], \quad (2)$$

where G_F is the Fermi constant and $V_{qq'}$ is the Cabibbo-Kobayashi-Maskawa (CKM) matrix element. After considering the factorizable contributions of $O_+^{qq'}$, the smallness of $\mathcal{B}(\Lambda_c^+ \rightarrow p\pi^0)$ is explained [49]. More importantly, Ref. [50] predicted that

$$\mathcal{B}(\Lambda_c^+ \rightarrow \Sigma^+ K_S^0) = \mathcal{B}(\Lambda_c^+ \rightarrow \Sigma^0 K^+), \quad (3)$$

$$\frac{\mathcal{B}(\Xi_c^0 \rightarrow \Sigma^0 K_S^0)}{\mathcal{B}(\Xi_c^0 \rightarrow \Xi^0 \pi^-)} = (2.3 \pm 1.8)\%, \quad (4)$$

which were not measured at that time. In particular, Eq. (3) is a critical prediction stemming from the KPW theorem and the modest ratio in Eq. (4) is quite surprising as both of them are Cabibbo favored (CF). These theoretical benchmarks have since been found consistent with recent experimental results [6,11].

In the present study, we build upon the framework established in Ref. [50], extending it to include the decays of Ω_c^0 and doubly charmed baryons. To accomplish this, we make two critical approximations:

- (1) We assume that the intermediate states are principally dominated by the low-lying baryons with spin-parity $\frac{1}{2}^+$ and $\frac{1}{2}^-$.
- (2) We posit that the flavor of the spectator quark exerts only a minimal influence on the baryon matrix elements.

It is worth noting that these approximations have been found to hold in the majority of model-dependent studies, and a detailed discussion on them will be provided later in this work.

This paper is structured in the following manner. In Sec. II, we delineate the $SU(3)_F$ representations of the charmed baryons. Section III is devoted to the evaluation of the factorizable contributions, utilizing the form factors derived from lattice QCD (LQCD). In Sec. IV, we thoroughly analyze the pole amplitudes and explore the dependencies on mass. Section V presents the numerical results, and finally, we conclude our findings in Sec. VI.

II. $SU(3)_F$ REPRESENTATION AND KÖRNER-PATI-WOO THEOREM

In general, the amplitudes of $\mathbf{B}_i \rightarrow \mathbf{B}_f P$ read

$$\mathcal{M} = \langle \mathbf{B}_f P; t \rightarrow \infty | \mathcal{H}_{\text{eff}} | \mathbf{B}_i \rangle = i\bar{u}_f (A + B\gamma_5) u_i, \quad (5)$$

where $u_{i(f)}$ is the Dirac spinor of the initial(final) baryon and $A(B)$ is the parity-violating(conserving) amplitude, corresponding to the $S(P)$ -partial wave. If the final state interaction is absent, one can freely interchange $t \rightarrow \pm\infty$ and A and B must be real. The decay width Γ and up-down asymmetry α are calculated by

$$\Gamma = \frac{p_f}{8\pi} \left(\frac{(M_i + M_f)^2 - M_P^2}{M_i^2} |A|^2 + \frac{(M_i - M_f)^2 - M_P^2}{M_i^2} |B|^2 \right),$$

$$\alpha = -\frac{2\kappa \text{Re}(A^* B)}{|A|^2 + \kappa^2 |B|^2}, \quad \kappa = \frac{p_f}{E_f + M_f}, \quad (6)$$

where $M_{i,f}$ and M_P are the masses of $\mathbf{B}_{i,f}$ and P , respectively and p_f and E_f are the magnitudes of the 3-momentum and energy of \mathbf{B}_f at the rest frame of \mathbf{B}_i .

To relate the decays with the $SU(3)_F$ symmetry, one has to write down the hadron representations in the $SU(3)_F$ group. We start with the low-lying pseudoscalar mesons. The responsible $SU(3)_F$ tensor is given by

$$P_j^i = \begin{pmatrix} \frac{1}{\sqrt{6}}\eta_8 + \frac{1}{\sqrt{2}}\pi^0 & \pi^+ & K^+ \\ \pi^- & \frac{1}{\sqrt{6}}\eta_8 - \frac{1}{\sqrt{2}}\pi^0 & K^0 \\ K^- & \bar{K}^0 & -\frac{2}{\sqrt{6}}\eta_8 \end{pmatrix}_{ij}, \quad (7)$$

which is related to the flavor part of wave functions according to

$$|P\rangle = P_j^i |q_i \bar{q}^j\rangle. \quad (8)$$

Here, the superscript and subscript of P_j^i describe the quark and antiquark flavors with $i, j \in \{1, 2, 3\}$ and $(q_1, q_2, q_3) = (u, d, s)$.

We exclusively consider the $SU(4)_F$ $\mathbf{20}$ multiplets, where the low-lying $\frac{1}{2}^+$ baryons are depicted in Fig. 1. We start with the idempotent of \square in the Young tableau, which projects out a subspace of the $SU(4)_F$ group, given by

$$e_{23} = (1 - (2, 3))(1 + (1, 2)), \quad (9)$$

where (1,2) interchange the first and second elements and (2,3) the second and third. For instance, we have

$$e_{23} |q_a q_b q_c\rangle = |q_a q_b q_c\rangle + |q_b q_a q_c\rangle - |q_a q_c q_b\rangle - |q_b q_c q_a\rangle. \quad (10)$$

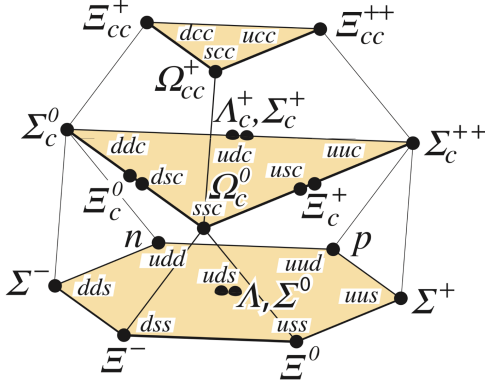


FIG. 1. The $SU(4)_F$ $\mathbf{20}$ multiplet represented by \boxplus [taken from the Particle Data Group (PDG) [1]].

It is clear that after operating e_{23} , states are antisymmetric in regard to the second and third quarks. The idempotent in Eq. (9) generates a subspace in the sense that $e_{23}e_A = e_{23}e_S = 0$, where $e_{S(A)}$ are the totally (anti)symmetric idempotent, given by

$$\begin{aligned} e_S &= 1 + (1,2) + (2,3) + (1,3) + (2,3)(1,2) + (1,2)(2,3), \\ e_A &= 1 - (1,2) - (2,3) - (1,3) + (2,3)(1,2) + (1,2)(2,3), \end{aligned} \quad (11)$$

We stress that throughout this work the $SU(4)_F$ representations are merely bookkeeping tools to unify the expressions and we do not take advantage of the $SU(4)_F$ symmetry.

If a light quark (u, d, s) pair is in antisymmetric, we utilize that the totally antisymmetric tensor ϵ^{ijk} is invariant under the $SU(3)_F$ transformation to simplify the indices, i.e., two antisymmetric quarks transform as an antiquark. As a result, the light quarks of \mathbf{B}_c^A are presented by one lower index as

$$(\mathbf{B}_c^A)_i = (\Xi_c^0, \Xi_c^+, \Lambda_c^+)_i. \quad (12)$$

Equation (12) can be translated back to a tensor with three quarks by

$$(\mathbf{B}_c^A)^{i[jk]} = \frac{1}{\sqrt{12}} (\mathbf{B}_c)_i (2\delta_4^i \epsilon^{ljk} + \delta_4^j \epsilon^{lik} - \delta_4^k \epsilon^{lij}), \quad (13)$$

with $q_4 = c$. Here, Eq. (13) is derived by

$$\begin{aligned} & e_{23} \frac{1}{\sqrt{12}} (|cud\rangle - |cdu\rangle) \\ &= \frac{1}{\sqrt{12}} (2|cud\rangle - 2|cdu\rangle + |ucd\rangle - |dcu\rangle \\ & \quad - |udc\rangle + |duc\rangle), \end{aligned} \quad (14)$$

where we have used Λ_c^+ as an instance. We start with $|cud\rangle - |cdu\rangle$ to make sure its isospin vanishes. One arrives at $|\Sigma_c^+\rangle$ if $|cud\rangle + |cdu\rangle$ is used instead.

On the other hand, the other low-lying baryons with spin-parity $\frac{1}{2}^+$ are

$$\begin{aligned} (\mathbf{B}_n)_j &= \begin{pmatrix} \frac{1}{\sqrt{6}}\Lambda + \frac{1}{\sqrt{2}}\Sigma^0 & \Sigma^+ & p \\ \Sigma^- & \frac{1}{\sqrt{6}}\Lambda - \frac{1}{\sqrt{2}}\Sigma^0 & n \\ \Xi^- & \Xi^0 & -\sqrt{\frac{2}{3}}\Lambda \end{pmatrix}_{ij}, \\ (\mathbf{B}_c^S)^{ij} &= \begin{pmatrix} \Sigma_c^{++} & \frac{1}{\sqrt{2}}\Sigma_c^+ & \frac{1}{\sqrt{2}}\Xi_c'^+ \\ \frac{1}{\sqrt{2}}\Sigma_c^+ & \Sigma_c^0 & \frac{1}{\sqrt{2}}\Xi_c'^0 \\ \frac{1}{\sqrt{2}}\Xi_c'^+ & \frac{1}{\sqrt{2}}\Xi_c'^0 & \Omega_c^0 \end{pmatrix}_{ij}, \\ (\mathbf{B}_{cc})^i &= (\Xi_{cc}^{++}, \Xi_{cc}^+, \Omega_{cc}^+)_i, \end{aligned} \quad (15)$$

where \mathbf{B}_c^S and \mathbf{B}_{cc} are the singly charmed sextet and doubly charmed baryons, respectively. Similarly, they are translated to tensors with three quark indices by

$$\begin{aligned} (\mathbf{B}_n)^{i[jk]} &= \frac{1}{\sqrt{2}} (\mathbf{B}_n)_i \epsilon^{ljk}, \\ (\mathbf{B}_c^S)^{i[jk]} &= \frac{1}{\sqrt{2}} ((\mathbf{B}_c)^{ij} \delta_4^k - (\mathbf{B}_c)^{ik} \delta_4^j), \\ (\mathbf{B}_{cc})^{i[jk]} &= \frac{1}{\sqrt{2}} ((\mathbf{B}_{cc})^j \delta_4^i \delta_4^k - (\mathbf{B}_{cc})^k \delta_4^i \delta_4^j), \end{aligned} \quad (16)$$

which would lead us to the convention in Ref. [3] up to some unphysical overall phase factors. In the quark model, the spin-flavor wave functions are obtained by

$$\begin{aligned} |\mathbf{B}\rangle &= (1 + (1,2) + (1,3)) \\ & \times \frac{\sqrt{2}}{3} [\mathbf{B}^{i[jk]} |q_i q_j q_k\rangle \otimes (|\uparrow\uparrow\downarrow\rangle - |\uparrow\downarrow\uparrow\rangle)], \end{aligned} \quad (17)$$

with $\mathbf{B} \in \{\mathbf{B}_n, \mathbf{B}_c^{A,S}, \mathbf{B}_{cc}\}$.

The effective Hamiltonian can be written in a compact way of

$$\mathcal{H}_{\text{eff}} = \frac{G_F}{\sqrt{2}} V_{ud} V_{cs}^* (\mathcal{H}_{kl}^{ij} (\bar{q}_i q^k)_{V-A} (\bar{q}_j q^l)_{V-A}), \quad (18)$$

where the nonzero elements are

$$\begin{aligned} \mathcal{H}_{24}^{13} &= c_1, & \mathcal{H}_{24}^{31} &= c_2, & \mathcal{H}_{34}^{13} &= c_1 s_c, & \mathcal{H}_{34}^{31} &= c_2 s_c, \\ \mathcal{H}_{24}^{12} &= -c_1 s_c, & \mathcal{H}_{24}^{21} &= -c_2 s_c, & \mathcal{H}_{34}^{12} &= -c_1 s_c^2, & \mathcal{H}_{34}^{21} &= -c_2 s_c^2, \end{aligned} \quad (19)$$

$s_c = V_{us}/V_{ud} = 0.23$, $c_1 = c_+ + c_-$, and $c_2 = c_+ - c_-$. Similar to the baryon states, one decomposes the effective Hamiltonian according to the permutation symmetry by

$$\mathcal{H}(\bar{\mathbf{6}})_{kl} \epsilon^{lij} = \frac{1}{c_-} (\mathcal{H}_{k4}^{ij} - \mathcal{H}_{k4}^{ji}), \quad \mathcal{H}(\mathbf{15})_k^{ij} = \frac{1}{2c_+} (\mathcal{H}_{k4}^{ij} + \mathcal{H}_{k4}^{ji}). \quad (20)$$

The factors of $1/c_-$ and $1/2c_+$ are included to match the convention. Comparing to Eq. (1), it is clear that $\mathcal{H}(\bar{\mathbf{6}})$ and $\mathcal{H}(\mathbf{15})$ take account O_- and O_+ in the effective Hamiltonian.

By far we have only considered the quark flavors and here is an appropriate place to further consider their colors also. With the Fierz transformation, it is straightforward to show that the color structure of \bar{q} and \bar{u} in $O_+^{qq'}$ is symmetric, and the same also applies to c and q' . Recall that baryons are antisymmetric in color, we arrive at

$$\langle q_a q_b q_c | O_+^{qq'} | \mathbf{B}_i \rangle = 0, \quad (21)$$

where the initial and final states are an arbitrary baryon and three-quark state, respectively. The same also applies to $\langle \mathbf{B}_f | O_+^{qq'} | q_a q_b q_c \rangle = 0$ with \mathbf{B}_f being the final-state baryon.

In the decays $\mathbf{B}_i \rightarrow \mathbf{B}_f P$, the nonfactorizable contributions can be approximated by the pole diagrams shown in Fig. 2, where the symbol \otimes marks the insertion of the effective Hamiltonian. This approximation results in the well-known KPW theorem, which states that O_+ contributes solely to the factorizable amplitudes. Notably, Eq. (21) is scale independent, as O_{\pm} do not undergo mixing in the

renormalization group evolution [63]. While a hard gluon exchange could challenge the KPW theorem, any breaking effect is likely below 10%. For a deeper dive into this topic, readers can consult Ref. [64]. There, the small branching fraction of $\mathcal{B}(B^0 \rightarrow p\bar{p})$ is attributed to a violation against the KPW theorem.¹ Since this deviation is even less significant than that of the $SU(3)_F$ breaking, we uphold the KPW theorem in this study.

To identify the factorizable contributions of O_+ , we observe the direct product of $\mathcal{H}(\mathbf{15})_k^{ij}$ and $(P^\dagger)_m^l$ has the representation of

$$\mathbf{15} \otimes \mathbf{8} = \mathbf{42} \oplus \bar{\mathbf{24}} \oplus \mathbf{15}_1 \oplus \mathbf{15}_1 \oplus \mathbf{15}_2 \oplus \bar{\mathbf{6}} \oplus \mathbf{3}. \quad (22)$$

The Hermitian conjugate is taken in P as it appears in the final states. The factorizable condition demands that the quark lines of P originate from O_+ exclusively. In other word, all the indices of $(P^\dagger)_m^l$ shall contract to the ones of $\mathcal{H}(\mathbf{15})_k^{ij}$. Symbolically it means that

$$\mathcal{H}(\mathbf{15})_k^{ij} \otimes (P^\dagger)_m^l = F^i \delta_m^j \delta_k^l, \quad (23)$$

where δ is the Kronecker delta, $F^i := \mathcal{H}(\mathbf{15})_k^{ij} (P^\dagger)_j^k$ and the other linear combinations do not contribute to $\mathbf{B}_i \rightarrow \mathbf{B}_f P$. It shows that only the $\mathbf{3}$ representation in Eq. (22) contributes, reducing numbers of free parameters.

By identifying the factorizable contribution, we reduce the number of free parameters from 14 to 8 for $\mathbf{B}_c^A \rightarrow \mathbf{B}_n P$ and arrive at [50]

$$A^{\mathbf{B}_c^A \rightarrow \mathbf{B}_n} = a_1^{\mathbf{B}_c^A} \mathcal{H}(\bar{\mathbf{6}})_{ij} T^{ik} (\mathbf{B}_n^\dagger)_k^l (P^\dagger)_l^j + a_2^{\mathbf{B}_c^A} \mathcal{H}(\bar{\mathbf{6}})_{ij} T^{ik} (P^\dagger)_k^l (\mathbf{B}_n^\dagger)_l^j + a_3^{\mathbf{B}_c^A} \mathcal{H}(\bar{\mathbf{6}})_{ij} (\mathbf{B}_n^\dagger)_k^i (P^\dagger)_l^j T^{kl} + a_6^{\mathbf{B}_c^A} (\mathbf{B}_n^\dagger)_i^j F^i (\mathbf{B}_c^A)_j, \quad (24)$$

where $T^{ij} \equiv (\mathbf{B}_c^A)_k \epsilon^{kij}$ and $a_{1,2,3,6}$ are free parameters in general. We note that we do not consider η' as its mass differs largely from the other pseudoscalar mesons. On the other hand, the \mathbf{B}_c^S and \mathbf{B}_{cc} decays are parametrized by

$$\begin{aligned} A^{\mathbf{B}_c^S \rightarrow \mathbf{B}_n} &= a_1^{\mathbf{B}_c^S} \mathcal{H}(\bar{\mathbf{6}})_{ij} (\mathbf{B}_c^S)_{ik} (\mathbf{B}_n^\dagger)_k^l (P^\dagger)_l^j + a_2^{\mathbf{B}_c^S} \mathcal{H}(\bar{\mathbf{6}})_{ij} (\mathbf{B}_c^S)_{ik} (P^\dagger)_k^l (\mathbf{B}_n^\dagger)_l^j + a_3^{\mathbf{B}_c^S} \mathcal{H}(\bar{\mathbf{6}})_{ij} (\mathbf{B}_n^\dagger)_k^i (P^\dagger)_l^j (\mathbf{B}_c^S)_{kl} \\ &+ a_4^{\mathbf{B}_c^S} \mathcal{H}(\bar{\mathbf{6}})_{ij} (\mathbf{B}_n^\dagger)_k^l (P^\dagger)_l^k (\mathbf{B}_c^S)_{ij} + a_6^{\mathbf{B}_c^S} (\mathbf{B}_n^\dagger)_k^j F^i (\mathbf{B}_c^S)_{kl} \epsilon_{ijl}, \end{aligned} \quad (25)$$

for $\mathbf{B}_c^S \rightarrow \mathbf{B}_n P$,

$$A^{\mathbf{B}_{cc} \rightarrow \mathbf{B}_c^A} = a_1^{\mathbf{B}_{cc} \rightarrow \mathbf{B}_c^A} (P^\dagger)_i^j (\mathbf{B}_c^{A\dagger})^i \mathcal{H}(\bar{\mathbf{6}})_{jk} (\mathbf{B}_{cc})^k + a_2^{\mathbf{B}_{cc} \rightarrow \mathbf{B}_c^A} (P^\dagger)_i^j (\mathbf{B}_c^{A\dagger})^k \mathcal{H}(\bar{\mathbf{6}})_{jk} (\mathbf{B}_{cc})^i + a_6^{\mathbf{B}_{cc} \rightarrow \mathbf{B}_c^A} F^i (\mathbf{B}_{cc})^j (\mathbf{B}_c^{A\dagger})^k \epsilon_{ijk}, \quad (26)$$

¹To be explicit, Ref. [64] shows that the amplitude of $B^0 \rightarrow p\bar{p}$ is proportional to c_+ instead of c_- .

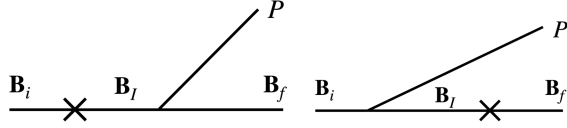


FIG. 2. The s - (left) and u -channels (right) of the pole contributions in $\mathbf{B}_i \rightarrow \mathbf{B}_f P$, where \times denotes the insertion of the effective Hamiltonian and \mathbf{B}_I is the intermediate state.

for $\mathbf{B}_{cc} \rightarrow \mathbf{B}_c^A P$, and

$$\begin{aligned} A^{\mathbf{B}_{cc} \rightarrow \mathbf{B}_c^S} &= a_1^{\mathbf{B}_{cc} \rightarrow \mathbf{B}_c^S} (P^\dagger)_i^j (\mathbf{B}_c^{S\dagger})_{jk} \mathcal{H}(\bar{\mathbf{6}})_{lm} (\mathbf{B}_{cc})^l \epsilon^{ikm} \\ &+ a_2^{\mathbf{B}_{cc} \rightarrow \mathbf{B}_c^S} (P^\dagger)_i^l (\mathbf{B}_c^{S\dagger})_{jk} \mathcal{H}(\bar{\mathbf{6}})_{lm} (\mathbf{B}_{cc})^j \epsilon^{ikm} \\ &+ a_6^{\mathbf{B}_{cc} \rightarrow \mathbf{B}_c^S} F^i (\mathbf{B}_{cc})^j (\mathbf{B}_c^{S\dagger})_{ij}, \end{aligned} \quad (27)$$

for $\mathbf{B}_{cc} \rightarrow \mathbf{B}_c^S P$. The P -wave amplitudes share the same flavor structures with the S -wave ones and are obtained by

$$B = A(a_{1,2,3,4,6} \rightarrow b_{1,2,3,4,6}). \quad (28)$$

The above parametrizations with (24)–(27) would be referred to as the general pole (GP) scenario. Up to date, only the decays of $\mathbf{B}_c^A \rightarrow \mathbf{B}_n P$ have sufficient experimental data points to fit $a_{1,\dots,6}^{\mathbf{B}_c^A}$. Given that our discussions on the GP scenario will be exclusively centered around $a_{1,\dots,6}^{\mathbf{B}_c^A}$ so confusion is not possible, we will omit their superscripts to maintain clarity.

One of the shortcoming of the GP scenario is that there are too many parameters. As there are few available input

for \mathbf{B}_c^S and \mathbf{B}_{cc} decays, the GP scenario does not have concrete predictions except for several direct relations. To overcome this problem, we assume that the intermediate baryons \mathbf{B}_I depicted in Fig. 2 are dominated by the low-lying ones, which would be referred to as the low-lying pole (LP) scenario. It allows us to infer the baryon matrix elements exhibited in $\mathbf{B}_c^S \rightarrow \mathbf{B}_n P$ and $\mathbf{B}_{cc} \rightarrow \mathbf{B}_c^{A,S} P$ from $\mathbf{B}_c^A \rightarrow \mathbf{B}_n P$. To this end, the next section is devoted to calculating the factorizable contributions, and in the section following the next one, we relate the four-quark operator matrix element in the decays of \mathbf{B}_{cc} and \mathbf{B}_c^A for evaluating the pole diagrams.

III. FACTORIZATION CONTRIBUTIONS

The amplitude is decomposed into the factorizable and nonfactorizable parts as

$$\mathcal{M} = \mathcal{M}^{\text{fac}} + \mathcal{M}^{\text{pole}}, \quad (29)$$

followed by $A = A^{\text{fac}} + A^{\text{pole}}$ and $B = B^{\text{fac}} + B^{\text{pole}}$. The factorizable amplitude reads

$$\mathcal{M}^{\text{fac}} = \frac{G_F}{\sqrt{2}} \tilde{\mathcal{H}}_{kl}^{ij} \langle P | \bar{q}_i \gamma_\mu (1 - \gamma_5) q^k | 0 \rangle \langle \mathbf{B}_f | \bar{q}_j \gamma^\mu (1 - \gamma_5) q^l | \mathbf{B}_i \rangle. \quad (30)$$

Expressing the baryon matrix element with the $SU(3)_F$ symmetry, we find

$$\begin{aligned} A^{\text{fac}} &= \frac{G_F}{\sqrt{2}} V_{cq}^* V_{uq} \mathcal{C}_{+,0} f_P (M_i - M_f) F_V \\ &= \frac{G_F}{\sqrt{2}} f_P (M_i - M_f) \tilde{\mathcal{H}}_{kl}^{ij} (P^\dagger)_i^k \left(A_1^{\text{fac}} \mathbf{B}^{m[nl]} \mathbf{B}_{m[nj]}^\dagger + A_2^{\text{fac}} \mathbf{B}^{m[nl]} \mathbf{B}_{n[jm]}^\dagger \right), \\ B^{\text{fac}} &= \frac{G_F}{\sqrt{2}} V_{cq}^* V_{uq} \mathcal{C}_{+,0} f_P (M_i + M_f) G_V, \\ &= \frac{G_F}{\sqrt{2}} f_P (M_i + M_f) \tilde{\mathcal{H}}_{kl}^{ij} (P^\dagger)_i^k \left(B_1^{\text{fac}} \mathbf{B}^{m[nl]} \mathbf{B}_{m[nj]}^\dagger + B_2^{\text{fac}} \mathbf{B}^{m[nl]} \mathbf{B}_{n[jm]}^\dagger \right), \end{aligned} \quad (31)$$

where $\mathcal{C}_{+,0}$ are the effective Wilson coefficients with the subscript denoting the charge of P , f_P is the meson decay constant, F_V and G_V are the leading vector and axial-vector form factors, respectively, $\tilde{\mathcal{H}}$ is obtained by substituting $\mathcal{C}_{+,0}$ for $c_{1,2}$ in Eq. (19), and \mathbf{B} and \mathbf{B}^\dagger are the tensors of \mathbf{B}_i and \mathbf{B}_f , respectively, given in Eqs. (13) and (16). From Eq. (17), we have $A_2^{\text{fac}}/A_1^{\text{fac}} = 1/2$ and $B_2^{\text{fac}}/B_1^{\text{fac}} = 5/4$.

For $c \rightarrow s$ and $c \rightarrow u/d$ transitions in $\mathbf{B}_c^{A,S}$ decays, we fix A_1^{fac} and B_1^{fac} with $\Lambda_c \rightarrow \Lambda$ and $\Lambda_c \rightarrow n$ from LQCD at $q^2 = 0$ [65–67],

$$\begin{aligned} (F_V, G_V)_{c \rightarrow s} &= (0.643, 0.572), \\ (F_V, G_V)_{c \rightarrow u/d} &= (0.672, 0.602), \end{aligned} \quad (32)$$

and arrive at

$$\begin{aligned} (A_1^{\text{fac}}, B_1^{\text{fac}})_{c \rightarrow s} &= (-2.572, -1.525), \\ (A_1^{\text{fac}}, B_1^{\text{fac}})_{c \rightarrow u/d} &= (-2.195, -1.311), \end{aligned} \quad (33)$$

where $q^\mu = p_i^\mu - p_f^\mu$ with $p_{i(f)}$ the 4-momentum of $\mathbf{B}_{i(f)}$. At the limit of the $SU(3)_F$ symmetry, the form factors of

$c \rightarrow s$ and $c \rightarrow u/d$ would be numerically the same. Here we see that they deviate roughly 15%, which is a common size of the $SU(3)_F$ breaking.

The form factors of $\mathbf{B}_{cc} \rightarrow \mathbf{B}_c^{A,S}$ from LQCD are not available yet. Nonetheless, we utilize the approximation that the form factors are independent of the spectator quark flavors, which allows us to infer them from $\Lambda_c^+ \rightarrow \Lambda/n$. This approximation is derived from the understanding that spectator quarks do not directly engage in the weak interaction. In Appendix A, we explore a few quark models as examples, demonstrating the spectator quarks have a negligible role.

The masses of \mathbf{B}_{cc} and $\mathbf{B}_c^{A,S}$ exhibit significant discrepancies. To circumvent the dependencies on mass inherent in the form factors, it is imperative to align the form factors using dimensionless variables. In this study, the form factors of $\mathbf{B}_{cc} \rightarrow \mathbf{B}_c^{A,S}$ are matched to those of $\mathbf{B}_c^A \rightarrow \mathbf{B}_n$ at an equivalent $\omega = v_i \cdot v_f$, where $v_{i(f)}$ symbolizes the 4-velocity of $\mathbf{B}_{i(f)}$. This ω is related to q^2 through the relation $\omega = \frac{M_i^2 + M_f^2 - q^2}{2M_i M_f}$. By using the form factors provided in Refs. [65,66], we arrive at

$$\begin{aligned} (A_1^{\text{fac}}, B_1^{\text{fac}})_{c \rightarrow s} &= (-3.615 - 1.939), \\ (A_1^{\text{fac}}, B_1^{\text{fac}})_{c \rightarrow d} &= (-3.518, -1.813), \end{aligned} \quad (34)$$

for $\mathbf{B}_{cc} \rightarrow \mathbf{B}_c^{A,S}$. The principal distinction between Eqs. (33) and (34) emerges due to the dependencies on ω within the form factors. Explicitly, for the transitions $\Xi_{cc}^{++} \rightarrow \Xi_c^+ \pi^+$ and $\Lambda_c^+ \rightarrow \Lambda \pi^+$, the values of $(\omega - 1)$ are 0.074 and 0.269, respectively, presenting a substantial deviation from one another. Given that the ω in $\mathbf{B}_{cc} \rightarrow \mathbf{B}_c^{A,S}$ is considerably smaller, a larger overlap in the wave functions is anticipated. Numerically, it is in accordance with Eqs. (33) and (34).

In this work, we fix $\mathcal{C}_0 = -0.36 \pm 0.04$ by $\mathcal{B}_{\text{exp}}(\Lambda_c^+ \rightarrow p\phi)$ from the experiment as shown in Appendix B while \mathcal{C}_+ is treated as a free parameter in general.

IV. POLE CONTRIBUTIONS

Consider the contribution of the pole in the s -channel as depicted in Fig. 2. When \mathbf{B}_I has negative parity, the amplitude can be expressed as

$$\mathcal{M}_s^{\text{pole}} = i\bar{u}_f g_{\mathbf{B}_f \mathbf{B}_I P} \frac{1}{p_i^\mu \gamma_\mu - M_I} (a_{\mathbf{B}_I \mathbf{B}_i} - b_{\mathbf{B}_I \mathbf{B}_i \gamma_5}) u_i, \quad (35)$$

where

$$\langle \mathbf{B}_I | \mathcal{H}_{\text{eff}} | \mathbf{B}_i \rangle = \bar{u}_I (a_{\mathbf{B}_I \mathbf{B}_i} - b_{\mathbf{B}_I \mathbf{B}_i \gamma_5}) u_i, \quad (36)$$

\mathbf{B}_I and M_I are the intermediate baryon and its corresponding mass, respectively, and the coupling of $\mathbf{B}_I - \mathbf{B}_f - P$ is denoted by $g_{\mathbf{B}_I \mathbf{B}_f P}$. Should \mathbf{B}_I exhibit positive parity, an additional γ_5 would follow $g_{\mathbf{B}_I \mathbf{B}_f P}$ in Eq. (35), a consequence of parity conservation in strong interaction. Similarly, the u -channel amplitude can be parametrized congruently to the expressions above.

In this work, the baryon-meson couplings of $g_{\mathbf{B}\mathbf{B}^{(*)}P}$ are extracted by the generalized Goldberg-Treiman relations

$$g_{\mathbf{B}'\mathbf{B}P} = \frac{\sqrt{2}}{f_P} (M' + M) g_{\mathbf{B}'\mathbf{B}}^P, \quad g_{\mathbf{B}^*\mathbf{B}P} = \frac{\sqrt{2}}{f_P} (M^* - M) g_{\mathbf{B}^*\mathbf{B}}^P, \quad (37)$$

where

$$\begin{aligned} (P^\dagger)_i^j \langle \mathbf{B}' | \bar{q}_i \gamma_\mu \gamma_5 q^j | \mathbf{B} \rangle &= \bar{u}_{\mathbf{B}'} (g_{\mathbf{B}'\mathbf{B}}^P \gamma_\mu - i g_2 \sigma_{\mu\nu} q^\nu + g_3 q_\mu) \gamma_5 u_{\mathbf{B}}, \\ (P^\dagger)_j^i \langle \mathbf{B}^* | \bar{q}_i \gamma_\mu \gamma_5 q^j | \mathbf{B} \rangle &= \bar{u}_{\mathbf{B}^*} (g_{\mathbf{B}^*\mathbf{B}}^P \gamma_\mu - i g_2 \sigma_{\mu\nu} q^\nu + g_3 q_\mu) u_{\mathbf{B}}. \end{aligned} \quad (38)$$

In this work, the symbols \mathbf{B}' and \mathbf{B}^* denote the intermediate baryons with spin-parity $\frac{1}{2}^+$ and $\frac{1}{2}^-$, respectively. The corresponding masses of $\mathbf{B}^{(\prime)}$ and \mathbf{B}^* are represented by $M^{(\prime)}$ and M^* . The Goldberg-Treiman relations are derived by operating q^μ on both sides of Eq. (38) and impose the equation of motion. The actual values of g_2 would be irrelevant to this work and g_3 is mainly contributed by the baryon-meson couplings.

Define the baryon matrix elements of the effective Hamiltonian with $\Delta c = -1$ as

$$\begin{aligned} \langle \mathbf{B}' | \mathcal{H}_{\text{eff}} | \mathbf{B} \rangle &= \bar{u}_{\mathbf{B}'} (a_{\mathbf{B}'\mathbf{B}} - b_{\mathbf{B}'\mathbf{B} \gamma_5}) u_{\mathbf{B}}, \\ \langle \mathbf{B}^* | \mathcal{H}_{\text{eff}} | \mathbf{B} \rangle &= \bar{u}_{\mathbf{B}^*} b_{\mathbf{B}^*\mathbf{B}} u_{\mathbf{B}}, \quad \langle \mathbf{B} | \mathcal{H}_{\text{eff}} | \mathbf{B}^* \rangle = \bar{u}_{\mathbf{B}} b_{\mathbf{B}\mathbf{B}^*} u_{\mathbf{B}^*}. \end{aligned} \quad (39)$$

In the following, $b_{\mathbf{B}'\mathbf{B}}$ will be dropped as it is tiny [68]. Collecting Eqs. (35), (37), and (39), we are led to

$$\begin{aligned} A^{\text{pole}}(\mathbf{B}_c \rightarrow \mathbf{B}_n P) &= \frac{\sqrt{2}}{f_P} \sum_{\mathbf{B}_{n,c}^*} (R_c^{A_s} g_{\mathbf{B}_n \mathbf{B}_{n,c}^*}^P b_{\mathbf{B}_{n,c}^* \mathbf{B}_c} + R_c^{A_u} b_{\mathbf{B}_n \mathbf{B}_{n,c}^*} g_{\mathbf{B}_{n,c}^* \mathbf{B}_c}^P), \\ B^{\text{pole}}(\mathbf{B}_c \rightarrow \mathbf{B}_n P) &= \frac{\sqrt{2}}{f_P} \sum_{\mathbf{B}_{n,c}} (R_c^{B_s} g_{\mathbf{B}_n \mathbf{B}_{n,c}}^P a_{\mathbf{B}_{n,c} \mathbf{B}_c} + R_c^{B_u} a_{\mathbf{B}_n \mathbf{B}_{n,c}} g_{\mathbf{B}_{n,c} \mathbf{B}_c}^P), \end{aligned} \quad (40)$$

and

$$\begin{aligned}
A^{\text{pole}}(\mathbf{B}_{cc} \rightarrow \mathbf{B}_c P) &= \frac{\sqrt{2}}{f_P} \sum_{\mathbf{B}'_{cc}} (R_{cc}^{A_s} g_{\mathbf{B}_c \mathbf{B}'_c}^P b_{\mathbf{B}'_c \mathbf{B}_{cc}} + R_{cc}^{A_u} b_{\mathbf{B}_c \mathbf{B}'_c} g_{\mathbf{B}'_c \mathbf{B}_{cc}}^P), \\
B^{\text{pole}}(\mathbf{B}_{cc} \rightarrow \mathbf{B}_c P) &= \frac{\sqrt{2}}{f_P} \sum_{\mathbf{B}'_{cc}} (R_{cc}^{B_s} g_{\mathbf{B}_c \mathbf{B}'_c}^P a_{\mathbf{B}'_c \mathbf{B}_{cc}} + R_{cc}^{B_u} a_{\mathbf{B}_c \mathbf{B}'_c} g_{\mathbf{B}'_c \mathbf{B}_{cc}}^P),
\end{aligned} \tag{41}$$

where the mass ratios are defined by

$$\begin{aligned}
R_c^{A_s} &= \frac{M_n - M_{n^*}}{M_c - M_{n^*}}, & R_c^{A_u} &= \frac{M_c - M_{c^*}}{M_{c^*} - M_n}, \\
R_c^{B_s} &= \frac{M_n + M_{n'}}{M_c - M_{n'}}, & R_c^{B_u} &= \frac{M_c + M_{c'}}{M_n - M_{c'}},
\end{aligned} \tag{42}$$

and

$$\begin{aligned}
R_{cc}^{A_s} &= \frac{M_c - M_{c^*}}{M_{cc} - M_{c^*}}, & R_{cc}^{A_u} &= \frac{M_d - M_{cc^*}}{M_{cc^*} - M_c}, \\
R_{cc}^{B_s} &= \frac{M_c + M_{c'}}{M_{cc} - M_{c'}}, & R_{cc}^{B_u} &= \frac{M_{cc} + M_{cc'}}{M_c - M_{cc'}}.
\end{aligned} \tag{43}$$

Here, $M_{n,c,cc^{(*)}}$ represent the masses of $\mathbf{B}_{n,c,cc}^{(*)}$, respectively.

Up to the present, there is no ample data to accurately fit the unknown hadronic parameters for Ω_c^0 and \mathbf{B}_{cc} decays. In the subsequent analysis, we will utilize two essential approximations, as delineated in the Introduction:

- (i) The intermediate states \mathbf{B}_I are exclusively confined to the low-lying $\mathbf{20}$ multiplets of the $SU(4)_F$ group. Here, $\mathbf{20} = \mathbf{8} \oplus \bar{\mathbf{3}} \oplus \mathbf{6} \oplus \mathbf{3}$ in the $SU(3)_F$ group.
- (ii) The baryon matrix elements are independent of the spectator quarks, implying that the amplitudes shown in Fig. 3 do not depend on $q^{(l)}$.

The reliability of our predictions hinges on the validity of these two approximations. The first approximation is grounded in that the low-lying states possess a larger overlap with \mathbf{B}_i and \mathbf{B}_f in Eq. (39), a convention widely adopted in the literature. It emphasizes that $\mathbf{B}' \in \{\mathbf{B}_c^{A,S}, \mathbf{B}_n, \mathbf{B}_{cc}\}$ and \mathbf{B}^* belong to the representation of $\mathbf{20}$ also.

On the other hand, we have already used the second approximation, discussed in Appendix A, to extract the form factors of $\mathbf{B}_{cc} \rightarrow \mathbf{B}_c^{A,S}$ in Eq. (34), which are

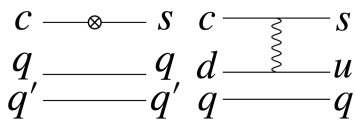


FIG. 3. The topological diagrams for the baryon matrix elements of the two-quark and four-quark operators. We use the approximation of that their magnitudes do not depend on $q^{(l)}$.

essentially two-quark operator matrix elements. The four-quark operators facilitate the parametrizations expressed in

$$\begin{aligned}
a_{\mathbf{B}'\mathbf{B}} &= \frac{4}{c_-} \tilde{a} \mathbf{B}^{i[jk]} \mathcal{H}_{jk}^{lm}(\mathbf{B}'^\dagger)_{i[lm]}, \\
b_{\mathbf{B}^*\mathbf{B}} &= \frac{4}{c_-} \tilde{b} \mathbf{B}^{i[jk]} \mathcal{H}_{jk}^{lm}(\mathbf{B}^{*\dagger})_{i[lm]}, \\
b_{\mathbf{B}\mathbf{B}^*} &= \frac{4}{c_-} \tilde{b}' (\mathbf{B}^*)^{i[jk]} \mathcal{H}_{jk}^{lm} \mathbf{B}_{i[lm]}^\dagger,
\end{aligned} \tag{44}$$

and

$$\begin{aligned}
g_{\mathbf{B}'\mathbf{B}}^P &= g_1 \mathbf{B}^{i[jk]}(\mathbf{B}'^\dagger)_{i[jl]} (P^\dagger)_k^l + g_2 \mathbf{B}^{i[jk]}(\mathbf{B}'^\dagger)_{j[l i]} (P^\dagger)_k^l, \\
g_{\mathbf{B}^*\mathbf{B}}^P &= g'_1 \mathbf{B}^{i[jk]}(\mathbf{B}^{*\dagger})_{i[jl]} (P^\dagger)_k^l + g'_2 \mathbf{B}^{i[jk]}(\mathbf{B}^{*\dagger})_{j[l i]} (P^\dagger)_k^l, \\
g_{\mathbf{B}\mathbf{B}^*}^P &= g'_1 \mathbf{B}_{i[jk]}^\dagger (\mathbf{B}^*)^{i[jl]} P_l^k + g'_2 \mathbf{B}_{l[ik]}^\dagger (\mathbf{B}^*)^{i[jl]} P_j^k.
\end{aligned} \tag{45}$$

Furthermore, by implementing Eq. (17), we obtain the ratio $g_2/g_1 = 5/4$, leading to the vanishing of $g_{\mathbf{B}'\mathbf{B}}^P$ [69]. Incorporating Eqs. (44) and (45) into Eqs. (40) and (41) and summing over \mathbf{B}_I , we eliminate the tensors of the intermediate states by employing the completeness relation [3],

$$\begin{aligned}
\sum_{\mathbf{B}_c^A} (\mathbf{B}_c^A)_i (\mathbf{B}_c^{A\dagger})^j &= \delta_i^j, & \sum_{\mathbf{B}_n} (\mathbf{B}_n)_i (\mathbf{B}_n^\dagger)_j &= \delta_i^j \delta_j^k - \frac{1}{3} \delta_i^k \delta_j^k, \\
\sum_{\mathbf{B}_{cc}} (\mathbf{B}_{cc})^i (\mathbf{B}_{cc}^\dagger)_j &= \delta_i^j, & \sum_{\mathbf{B}_c^S} (\mathbf{B}_c^S)^{ij} (\mathbf{B}_c^{S\dagger})_{kl} &= \frac{1}{2} (\delta_k^i \delta_l^j + \delta_k^j \delta_l^i),
\end{aligned} \tag{46}$$

where we have taken the baryons with spin-parity $\frac{1}{2}^+$ as examples. The same relation would hold for $\mathbf{B}_{n,c,cc}^*$ as they belong to the same $SU(3)_F$ group, which allows us to consider the contributions of negative baryons without specifying them. A concrete example will be provided in the next section.

To calculate $R_{c,cc}^{B_{s,u}}$, the masses of $\mathbf{B}^{(*)}$ are accessible from experimental measurements [1]. However, the masses of \mathbf{B}^* are not fully available yet. For the charmless octet baryons, we consider the states $N(1535)$ and $\Sigma(1750)$, taking the average mass value of $M_{n^*} = 1643$ MeV. For the charmed

baryons with negative parity \mathbf{B}_c^* , we identify the candidates as $\Lambda_c^+(2595)$, $\Xi_c^+(2790)$, and $\Sigma_c^+(2792)$, from which we calculate the average masses $M_{c^*} = 2700$ MeV and $M_{c^*} = 2900$ MeV for the $\bar{\mathbf{3}}$ and $\mathbf{6}$ representations, respectively. In the case of the doubly charmed baryons with $J = \frac{1}{2}^-$, we adopt the value $M_{cc^*} = 3932$ MeV [70]. Summarizing, the mass ratios related to the $J = \frac{1}{2}^-$ baryons utilized in this work are expressed as

$$\begin{aligned} (R_c^{A_s}, R_c^{A_u}(\bar{\mathbf{3}}), R_c^{A_u}(\mathbf{6})) &= (-0.671, -0.207, -0.298), \\ (R_{cc}^{A_s}(\bar{\mathbf{3}}), R_{cc}^{A_s}(\mathbf{6}), R_{cc}^{A_u}) &= (-0.350, -0.725, -0.201), \end{aligned} \quad (47)$$

where the parenthesis denotes the representation of M_{c^*} . We note that focusing solely on \mathbf{B}_c^A decays, the uncertainties in $R_{c,cc}^{A_{s,u}}$ would be incorporated into the baryon matrix elements of $g'_{1,2}$ and $\tilde{b}^{(\prime)}$. Consequently, the errors in Eq. (47) would only influence the predictions for the Ω_c^0 and \mathbf{B}_{cc} decays.

V. NUMERICAL RESULTS

The parametrized expressions of the LP scenario are given in Appendix C. Since $g_{\mathbf{B}^* \mathbf{B}}^P (g_{\mathbf{B}^* \mathbf{B}}^P)$ is always followed by $a_{\mathbf{B}^* \mathbf{B}} (b_{\mathbf{B}^* \mathbf{B}})$, we absorb $g_1 (g'_1)$ into $\tilde{a} (\tilde{b}^{(\prime)})$ so that $g_1^{(\prime)} = 1$. For the nonfactorizable amplitudes, there remain (\tilde{a}) and $(\tilde{b}, \tilde{b}', g'_2)$ to be fitted in the P - and S -waves, respectively.

The numerical results of this study are organized into several subsections. In Sec. VA, we recall the experimental data of the \mathbf{B}_c^A decays, and the free parameters in both the LP and GP scenarios are extracted accordingly. Although the GP scenario provides more reliable predictions for \mathbf{B}_c^A decays, the LP scenario has broader applications, i.e., its parameters can be applied to both Ω_c^0 and \mathbf{B}_{cc} decays. Sections VB and VC are devoted to the study of Ω_c^0 and \mathbf{B}_{cc} decays in the LP scenario, respectively.

A. Results of \mathbf{B}_c^A decays

We take $\Lambda_c^+ \rightarrow \Lambda \pi^+$ as a concrete example for the LP scenario. Plugging the $SU(3)_F$ tensors of Λ_c^+, Λ and π^+ into Eq. (31), we arrive at

$$\begin{aligned} A^{\text{fac}}(\Lambda_c^+ \rightarrow \Lambda \pi^+) &= \frac{G_F}{\sqrt{2}} V_{cs} V_{ud} (M_{\Lambda_c} - M_{\Lambda}) f_{\pi} \\ &\times C_+ \left(-\frac{A_1}{6} - \frac{A_2}{6} \right), \end{aligned} \quad (48)$$

while the P -wave share the same $SU(3)_F$ structure with the S -wave and can be obtained by the substitution of

$$B^{\text{fac}} = A^{\text{fac}}(M_i - M_f \rightarrow M_i + M_f, A_{1,2} \rightarrow B_{1,2}). \quad (49)$$

Notice that we have $A_2 = A_1/2$ and $B_2 = 5B_1/4$. The second parenthesis in Eq. (48) corresponds to the form factors of $\Lambda_c \rightarrow \Lambda$ and A_1 and B_1 are given in Eq. (33). In the global fit, the Fermi constant, CKM matrix elements and hadron masses are taken from PDG and the decay constants are taken to be $(f_{\pi}, f_K, f_{\eta}) = (130, 156, 162)$ in units of MeV. The effective Wilson coefficient for the charged meson C_+ is treated as a free parameter. On the other hand, the S -wave pole contribution is given by Eq. (40)

$$\begin{aligned} A^{\text{pole}}(\Lambda_c^+ \rightarrow \Lambda \pi^+) &= \frac{\sqrt{2}}{f_{\pi}} \sum_{\mathbf{B}_{n,c}} (R_c^{A_s} g_{\Lambda \mathbf{B}_n}^{\pi^+} b_{\mathbf{B}_n \Lambda_c^+} + R_c^{A_u} b_{\Lambda \mathbf{B}_n} g_{\mathbf{B}_n \Lambda_c^+}^{\pi^+}). \end{aligned} \quad (50)$$

The mass inputs of $R_c^{A_s}$ and $R_c^{A_u}$ are given in Eq. (47). The dependency on $\mathbf{B}_{c,n}$ can be summed over by using the completeness relations. We take the first term in Eq. (50) as an example. Plugging in Eqs. (44) and (45), we arrive at

$$\begin{aligned} \sum_{\mathbf{B}_n^*} g_{\Lambda \mathbf{B}_n}^{\pi^+} b_{\mathbf{B}_n \Lambda_c^+} &= \frac{4}{c_-} \sum_{\mathbf{B}_n^*} (g'_1 \Lambda_{i[jk]}^{\dagger} (\pi^-)_i^k + g'_2 \Lambda_{l[ik]}^{\dagger} (\pi^-)_j^k) (\mathbf{B}_n^*)^{i[jl]} \tilde{b} (\Lambda_c^+)^{m[op]} \mathcal{H}_{op}^{qr} (\mathbf{B}_n^{*\dagger})_{mqr} \\ &= \frac{4}{c_-} (\Lambda_{i[jk]}^{\dagger} (\pi^-)_i^k + g'_2 \Lambda_{l[ik]}^{\dagger} (\pi^-)_j^k) \tilde{b} (\Lambda_c^+)^{m[op]} \mathcal{H}_{op}^{qr} \sum_{\mathbf{B}_n} \frac{1}{2} (\mathbf{B}_n^*)_s^i \epsilon^{sjl} (\mathbf{B}_n^{*\dagger})_m^t \epsilon_{tqr} \\ &= \frac{4}{c_-} (\Lambda_{i[jk]}^{\dagger} (\pi^-)_i^k + g'_2 \Lambda_{l[ik]}^{\dagger} (\pi^-)_j^k) \tilde{b} (\Lambda_c^+)^{m[op]} \mathcal{H}_{op}^{qr} \epsilon^{sjl} \epsilon_{tqr} \frac{1}{2} \left(\delta_m^i \delta_s^t - \frac{1}{3} \delta_s^i \delta_m^t \right) \\ &= \tilde{b} \left(\frac{2}{3} g'_2 - \frac{1}{3} \right). \end{aligned} \quad (51)$$

We used Eq. (16) in the third line and absorbed g'_1 into \tilde{b} by redefinition explained previously. The completeness relation in Eq. (46) for \mathbf{B}_n^* has been used in the fourth line. The derivation is quite tedious but can be done straightforwardly by a computer program. Repeating similar processes, we arrive at

$$A^{\text{pole}}(\Lambda_c^+ \rightarrow \Lambda \pi^+) = \frac{\sqrt{2}}{f_{\pi}} \left[R_c^{A_s} \tilde{b} \left(\frac{2}{3} g'_2 - \frac{1}{3} \right) + R_c^{A_u}(\mathbf{6}) \tilde{b}' \left(\frac{2}{3} g'_2 - \frac{1}{3} \right) \right], \quad (52)$$

As the intermediate baryons with $J^P = \frac{1}{2}^\pm$ are both represented by $\mathbf{20}$, B^{pole} can be obtained by the substitutions of

$$B^{\text{pole}} = A^{\text{pole}} \left(\tilde{b} \rightarrow \tilde{a}, \tilde{b}' \rightarrow \tilde{a}, g_2 \rightarrow \frac{5}{4}, R_c^{A_s,u} \rightarrow R_c^{B_s,u} \right). \quad (53)$$

Collecting Eqs. (48), (49), (52), and (53) would complete the analysis of $\Lambda_c^+ \rightarrow \Lambda$ and $(C_+, \tilde{b}, \tilde{b}', g_2, \tilde{a})$ remain free parameters to be fitted.

Comparing to the GP scenario [50], the parameters of the nonfactorizable amplitudes in the P -waves have been reduced from 3 to 1. It is due to that we have related $g_{\mathbf{B}_n \mathbf{B}'_n}^P$ with $g_{\mathbf{B}_c \mathbf{B}'_c}^P$ in Eq. (45) and demand $4g_2 = 5g_1$. On the other hand, due to a lack of knowledge of parity-odd

baryons, we impose no further constraints on the S -waves in comparison to the GP scenario. The equivalence between the GP and LP scenarios in S -waves for pole contributions can be seen explicitly by the matching of

$$\begin{aligned} a_1^{\text{fac}} &= a_3^{\text{fac}} = \frac{G_F}{\sqrt{2}} V_{cs}^* V_{ud} f_P (C_+ - C_0) \frac{(A_1 + A_2)}{8\sqrt{6}}, \\ a_2^{\text{fac}} &= 0, \\ a_6^{\text{fac}} &= \frac{G_F}{\sqrt{2}} V_{cs}^* V_{ud} f_P (C_+ + C_0) \frac{(A_1 + A_2)}{4\sqrt{6}}, \end{aligned} \quad (54)$$

and

$$\begin{aligned} a_1^{\text{pole}} &= \frac{\sqrt{2}}{f_P} \left(\frac{\sqrt{6}}{6} R_c^{A_s} \tilde{b} (g_1 - g_2) \right), \\ a_2^{\text{pole}} &= -\frac{\sqrt{2}}{f_P} \left(\frac{6R_c^{A_s} \tilde{b} g_2 + R_c^{A_u} (\bar{\mathbf{3}}) \tilde{b}' (5g_1 - 4g_2) - 3R_c^{A_u} (\mathbf{6}) \tilde{b}' (g_1 - 2g_2)}{6\sqrt{6}} \right), \\ a_3^{\text{pole}} &= -\frac{\sqrt{2}}{f_P} \left(\frac{\tilde{b}' R_c^{A_u} (\bar{\mathbf{3}}) (5g_1 - 4g_2) + 3\tilde{b}' R_c^{A_u} (\mathbf{6}) (g_1 - 2g_2)}{6\sqrt{6}} \right), \\ a_6^{\text{pole}} &= 0. \end{aligned} \quad (55)$$

Here we have decomposed $a_i = a_i^{\text{fac}} + a_i^{\text{pole}}$. Using Eqs. (49) and (53), we find similar relations in P -waves.

The experimental data regarding the decays of \mathbf{B}_c^A are summarized in Table I [1,7,12]. We employed the minimal χ^2 fitting method with the 22 observables outlined in Table I to fit $(\tilde{a}, \tilde{b}, \tilde{b}', g_2, C_+)$ and arrive at the following results:

$$(\tilde{a}, \tilde{b}, \tilde{b}', g_2, C_+) = (2.06 \pm 0.25, 12.51 \pm 1.03, -4.01 \pm 1.13, 0.148 \pm 0.075, 0.467 \pm 0.034), \quad (56)$$

where the units for $(\tilde{a}, \tilde{b}, \tilde{b}')$ are $10^{-3} G_F \text{ GeV}^3$. The uncertainties in Eq. (56) originate from experimental input. A succinct overview of the minimal χ^2 method is given in Appendix D. In this study, we do not account for potential additional uncertainties that may arise due to the complexities in hadronic interactions.

In the limit of the $SU(4)_F$ symmetry, we would expect $\tilde{b} = \tilde{b}'$, but we observe a significant $SU(4)_F$ breaking as

they differ both in sign and magnitude. It indicates that the charm quark and the light quarks behave very differently in \mathbf{B}^* . We note that C_+ is twice smaller than the expected value of $C_+ \approx 1.2$ from the effective color number approach, discussed in Appendix B.

For comparison, we also update the results of the GP scenario. The free parameters in Eq. (24) with the same experimental input in Table I are found to be

$$\begin{aligned} (a_1, a_2, a_3, a_6) &= (3.25 \pm 0.11, 1.60 \pm 0.07, 0.58 \pm 0.12, 1.74 \pm 0.22), \\ (b_1, b_2, b_3, b_6) &= (11.66 \pm 0.19, -4.96 \pm 0.19, 2.87 \pm 0.27, -0.03 \pm 0.36), \end{aligned} \quad (57)$$

in units of $10^{-2} G_F \text{ GeV}^2$. Comparing to the previous values,² we see that the parameters modify significantly. It is a hint of that the results shall not be trust fully. Since the $SU(3)_F$ symmetry is not exact and too many parameters are required, it is reasonable that the best-fitting solutions are not stable along with the experimental update.

²With the experimental data up to May 16, 2019, Ref. [50] reported $(a_1, a_2, a_3, a_6) = (4.34 \pm 0.50, -1.33 \pm 0.32, 1.25 \pm 0.36, -0.26 \pm 0.64)$ and $(b_1, b_2, b_3, b_6) = (9.20 \pm 2.09, 8.03 \pm 1.19, -1.42 \pm 1.61, 4.05 \pm 2.48)$ instead.

TABLE I. Results of the low-lying and general pole scenarios, denoted with LP and GP in the subscripts, where the parameters are extracted from the current experimental data of \mathcal{B}_{exp} and α_{exp} collected in the first column [1,7,12]. Here, the numbers in the parentheses are the uncertainties counting backward in digits, for example, $1.59(8) = 1.59 \pm 0.08$.

Channels	$\mathcal{B}_{\text{exp}}(\%)$	α_{exp}	$\mathcal{B}_{LP}(\%)$	α_{LP}	$\mathcal{B}_{GP}(\%)$	α_{GP}
$\Lambda_c^+ \rightarrow pK_S^0$	1.59(8)	0.18(45)	1.44(7)	-0.68(1)	1.55(6)	-0.81(5)
$\Lambda_c^+ \rightarrow \Lambda\pi^+$	1.30(6)	-0.755(6)	0.96(16)	-0.75(1)	1.32(5)	-0.75(1)
$\Lambda_c^+ \rightarrow \Sigma^0\pi^+$	1.27(6)	-0.466(18)	1.14(14)	-0.45(4)	1.25(5)	-0.47(1)
$\Lambda_c^+ \rightarrow \Sigma^+\pi^0$	1.25(10)	-0.48(3)	1.14(14)	-0.45(4)	1.25(5)	-0.47(1)
$\Lambda_c^+ \rightarrow \Xi^0 K^+$	0.55(7)		0.02(2)	-0.02(0)	0.41(3)	0.95(2)
$\Lambda_c^+ \rightarrow \Lambda K^+$	0.064(3)	-0.585(52)	0.072(8)	-0.76(4)	0.065(3)	-0.56(4)
$\Lambda_c^+ \rightarrow \Sigma^0 K^+$	0.0382(25)	-0.54(20)	0.028(3)	-0.41(5)	0.039(2)	-1.00(0)
$\Lambda_c^+ \rightarrow n\pi^+$	0.066(13)		0.008(5)	-0.87(11)	0.067(3)	0.53(5)
$\Lambda_c^+ \rightarrow \Sigma^+ K_S^0$	0.047(14)		0.028(3)	-0.41(5)	0.039(2)	-1.00(0)
$\Lambda_c^+ \rightarrow p\pi^0$	$< 8 \times 10^{-3}$		0.01(1)	-0.77(24)	0.01(0)	0.92(8)
${}^a\Lambda_c^+ \rightarrow p\eta$	0.158(12)		0.142(8)	-0.70(1)	0.150(8)	-0.45(10)
${}^a\Lambda_c^+ \rightarrow \Sigma^+\eta$	0.312(44)	-0.99(6)	0.13(3)	-0.49(10)	0.35(2)	-0.47(5)
$\Xi_c^+ \rightarrow \Xi^0\pi^+$	1.6(80)		0.87(18)	-0.88(7)	0.87(8)	-0.88(4)
$\Xi_c^0 \rightarrow \Lambda K_S^0$	0.32(7)		0.54(3)	-0.61(2)	0.68(2)	-0.69(4)
$\Xi_c^0 \rightarrow \Xi^-\pi^+$	1.43(32)	-0.64(5)	2.98(29)	-0.64(2)	2.98(8)	-0.99(0)
$\Xi_c^0 \rightarrow \Xi^- K^+$	0.039(12)		0.135(14)	-0.69(1)	0.131(4)	-0.97(0)
$\Xi_c^0 \rightarrow \Sigma^0 K_S^0$	0.054(16)		0.057(13)	-0.91(5)	0.053(16)	0.59(13)
$\Xi_c^0 \rightarrow \Sigma^+ K^-$	0.18(4)		0.01(2)	-0.27(11)	0.48(3)	1.00(0)

^aThe experimental branching fractions are not included in the global fit.

In regard to the results in Table I, several comments are in order:

- (i) For $\alpha(\Lambda_c^+ \rightarrow pK_S)$, $\mathcal{B}(\Xi_c^0 \rightarrow \Lambda K_S)$, and especially $\mathcal{B}(\Xi_c^0 \rightarrow \Xi^-\pi^+)$, good accordance is found in two scenarios but both suggest very different values against the current experimental data. It indicates that the short distance contributions may play a dominate role in these decays. Experimental revisits on these channels will be welcome.
- (ii) The results of $\Lambda_c^+ \rightarrow \Xi^0 K^+$, $\Lambda_c^+ \rightarrow n\pi^+$, and $\Xi_c^0 \rightarrow \Sigma^+ K^-$ deviate largely between two scenarios. It implies that the excited states which do not belong to the $20SU(4)_F$ multiplets may play an important role in P -waves since the parametrizations of two scenarios are equivalent in S -waves.
- (iii) The P -wave amplitude of $\Lambda_c^+ \rightarrow \Xi^0 K^+$ vanishes naturally in the LP scenario [3], resulting in $\alpha_{LP} = 0$. Nonetheless, $\alpha_{GP} = 0.95 \pm 0.02$ indicates another way round.
- (iv) In contrast to the P -wave, the S -wave does not vanish in general for $\Lambda_c^+ \rightarrow \Xi^0 K^+$ in the LP scenario. However, the current experimental data prefers a vanishing S -wave also, leading to contradiction against $\mathcal{B}_{\text{exp}}(\Lambda_c^+ \rightarrow \Xi^0 K^+)$.
- (v) Continuing the above comment, we see that the LP scenario also fails to explain $\mathcal{B}_{\text{exp}}(\Lambda_c^+ \rightarrow n\pi^+)$, but $\mathcal{B}_{GP}(\Lambda_c^+ \rightarrow \Xi^0 K^+)$ and $\mathcal{B}_{GP}(\Lambda_c^+ \rightarrow n\pi^+)$ are consistent with the experimental data.

- (vi) The ratio of $\mathcal{R}_{K/\pi} := \mathcal{B}(\Xi_c^0 \rightarrow \Xi^- K^+)/\mathcal{B}(\Xi_c^0 \rightarrow \Xi^- \pi^+)$ is fixed in the exact $SU(3)_F$ symmetry. From the GP and LP scenarios, we find $\mathcal{R}_{K/\pi} = 4.5\%$ and $\mathcal{R}_{K/\pi} = 4.4\%$, respectively, which both contradict to the experimental value of $(2.75 \pm 0.51 \pm 0.25)\%$ at Belle [9].
- (vii) We do not include $\mathcal{B}_{\text{exp}}(\Lambda_c^+ \rightarrow p\eta)$ and $\mathcal{B}_{\text{exp}}(\Lambda_c^+ \rightarrow \Sigma^+\eta)$ into the global fit as we do not consider the $SU(3)_F$ singlet in P . The results of this work are obtained by assuming the mixing between η_0 and η_8 is absent. Surprisingly, the numerical results turn out to be compatible with the current experimental data.

It is insightful to compare the LP scenario with Ref. [38] which computes the S -wave amplitudes by the soft meson approximation. Comparisons for several chosen channels are collected in Table II. The factorizable amplitudes with the neutral P agree well as they are fixed by $\mathcal{B}_{\text{exp}}(\Lambda_c^+ \rightarrow p\phi)$. However, for $\Lambda_c^+ \rightarrow \Lambda\pi^+$ our A^{fac} and B^{fac} are roughly twice smaller than Ref. [38] as we adopt a much smaller \mathcal{C}_+ , and we find a sizable A^{pole} in contrast to $A^{\text{pole}} = 0$ at the soft meson limit. One possible explanation to reconcile two approaches is that a sizable proportion from excited intermediate baryons is reabsorbed into \mathcal{C}_+ , leading to a smaller value of $\mathcal{C}_+ = 0.469$ against the naive expectation of $\mathcal{C}_+ \approx 1$. We see that although our sizes of the S - and P -wave amplitudes differ with Ref. [38], the signs

TABLE II. Comparison between the LP scenario and the current algebra approach [38], where A and B are in units of $10^{-2}G_F \text{ GeV}^2$.

Channels	LP scenario				Current algebra [38]			
	A^{fac}	A^{pole}	B^{fac}	B^{pole}	A^{fac}	A^{pole}	B^{fac}	B^{pole}
$\Lambda_c^+ \rightarrow \Sigma^+ \pi^0$	0	-5.82	0	-4.47	0	-7.68	0	-11.34
$\Lambda_c^+ \rightarrow \Sigma^+ \eta$	0	2.16	0	2.04	0	3.10	0	15.54
$\Lambda_c^+ \rightarrow \Sigma^0 \pi^+$	0	5.81	0	4.44	0	7.68	0	11.38
$\Lambda_c^+ \rightarrow \Xi^0 K^+$	0	-0.79	0	-0.04	0	-4.48	0	12.10
$\Lambda_c^+ \rightarrow p \bar{K}^0$	3.91	5.31	8.38	0.74	3.45	4.48	6.98	2.06
$\Lambda_c^+ \rightarrow \Lambda \pi^+$	3.16	1.84	8.18	-1.60	5.34	0	14.11	-3.60
$\Lambda_c^+ \rightarrow p \pi^0$	0.53	-0.30	1.14	-0.88	0.41	-0.81	0.87	-2.07
$\Lambda_c^+ \rightarrow n \pi^+$	0.87	-0.43	1.88	-1.24	1.64	-1.15	3.45	-2.93
$\Xi_c^+ \rightarrow \Sigma^+ \bar{K}^0$	3.70	-0.76	9.51	-4.46	2.98	-4.48	9.95	-12.28
$\Xi_c^+ \rightarrow \Xi^0 \pi^+$	-3.81	0.92	-11.13	5.49	-7.41	5.36	-28.07	14.03
$\Xi_c^0 \rightarrow \Sigma^+ K^-$	0	0.79	0	0.33	0	4.42	0	-12.09
$\Xi_c^0 \rightarrow \Sigma^0 \bar{K}^0$	2.62	-1.09	6.73	-3.39	2.11	-3.12	7.05	-9.39
$\Xi_c^0 \rightarrow \Xi^0 \pi^0$	0	5.15	0	4.62	0	7.58	0	11.79
$\Xi_c^0 \rightarrow \Xi^0 \eta$	0	-3.12	0	-2.41	0	10.80	0	-6.17
$\Xi_c^0 \rightarrow \Xi^- \pi^+$	-3.80	-6.37	-11.16	-1.04	-7.42	-5.36	-28.24	-2.65
$\Xi_c^0 \rightarrow \Lambda \bar{K}^0$	1.60	4.97	3.80	2.45	1.11	5.41	3.66	6.87

are consistent for most of the cases. We point out that good agreements in $\Lambda_c^+ \rightarrow p \pi^0$ and $\Lambda_c^+ \rightarrow n \pi^+$ with Ref. [38] are found, where large destructive interference between factorizable and pole amplitudes occurs. It indicates that the current algebra approach with the soft-meson limit is a good approximation for describing the low-lying poles. However, it shall be noted that the LP scenario and Ref. [38] both obtain a much smaller $\mathcal{B}(\Lambda_c^+ \rightarrow n \pi^+)$ comparing to the experiments [8].³

The numerical results of the \mathbf{B}_c^A decay channels, for which there are no experimental references yet, are collected in Appendix E for use in future experiments as a basis for verification.

B. Results of Ω_c^0 decays

Lacking of experimental input, the GP scenario is not available for Ω_c^0 decays. Based on the LP scenario, the predictions of $\Omega_c^0 \rightarrow \mathbf{B}_n P$ are collected in Table III, where the lifetime of Ω_c^0 is taken to be (273 ± 12) fs [1]. It is interesting to see that $\mathcal{B}(\Omega_c^0 \rightarrow \Xi^0 K_S^0)$ and $\mathcal{B}(\Omega_c^0 \rightarrow K_L^0)$ deviate significantly, induced by the interference between the CF and doubly Cabibbo suppressed (DCS) amplitudes.

In Table IV, we compare our predictions for Cabibbo suppressed (CS) decays with those from the current algebra [35]. Our results are in good agreement for $\Omega_c^0 \rightarrow \Xi^0 \pi^0$ and $\Omega_c^0 \rightarrow \Xi^- \pi^+$, but they deviate significantly for $\Omega_c^0 \rightarrow \Sigma^+ K^-$ and $\Omega_c^0 \rightarrow \Lambda \bar{K}^0$. Particularly, our $\mathcal{B}(\Omega_c^0 \rightarrow \Sigma^+ K^-)$ is four

times smaller. Future experimental investigations could resolve this issue.

Up to date, the measurements of the Ω_c^0 decay ratios are performed in regard to $\Omega_c^0 \rightarrow \Omega^- \pi^+$. Fortunately, $\Omega_c^0 \rightarrow \Omega^- \pi^+$ does not receive W -exchange contributions and is color-enhanced. The branching fraction is calculated by

$$\Gamma = \frac{P_f}{16\pi M_{\Omega_c}^2} (|H_+^{\text{fac}}|^2 + |H_-^{\text{fac}}|^2), \quad (58)$$

where H_+^{fac} and H_-^{fac} are the factorizable helicity amplitudes defined as

$$H_{\pm} = \frac{G_F}{\sqrt{2}} V_{cs}^* V_{ud} C'_+ f_{\pi} q^{\mu} \times \left\langle \Omega^-; \lambda = \pm \frac{1}{2} \left| \bar{s} \gamma_{\mu} (1 - \gamma_5) c \right| \Omega_c; J_z = \pm \frac{1}{2} \right\rangle, \quad (59)$$

$q^{\mu} = (q^0, 0, 0, -q^3)$ is the four-momentum of the pion, λ and J_z are the helicity and angular momentum of Ω^- and Ω_c^0 , respectively, and C'_+ is the responsible effective Wilson coefficient. In this work, the baryonic matrix elements in Eq. (59) are evaluated from the homogeneous bag model [71].

As Ω^- does not belong to the $\mathbf{20}$ $SU(4)_F$ multiplets, $\Omega_c^0 \rightarrow \Omega^- \pi^+$ does not necessarily share the same effective Wilson coefficients with $\mathcal{B}_c^{A,S} \rightarrow \mathbf{B}_n P$. In Table V, we compare the outcomes with various C'_+ , where

$$\mathcal{R}(\Omega_c^0 \rightarrow \mathbf{B}_n P) := \frac{\mathcal{B}(\Omega_c^0 \rightarrow \mathbf{B}_n P)}{\mathcal{B}(\Omega_c^0 \rightarrow \Omega^- \pi^+)}, \quad (60)$$

³Reference [38] obtains $\mathcal{B}(\Lambda_c^+ \rightarrow n \pi^+) = 9 \times 10^{-5}$ in accordance with $(8 \pm 5) \times 10^{-5}$ in the LP scenario.

TABLE III. Predictions of the CF, CS, and DCS decays with Ω_c^0 as the initial baryons, where A and B are in units of $10^{-2}G_F \text{ GeV}^2$.

CF decays	A^{fac}	A^{pole}	B^{fac}	B^{pole}	$\mathcal{B}(\%)$	α
$\Omega_c^0 \rightarrow \Xi^0 K_S^0$	-2.43	0.54	2.11	-5.46	0.22(5)	-0.86(10)
$\Omega_c^0 \rightarrow \Xi^0 K_L^0$	2.19	-1.24	-1.90	5.57	0.11(3)	-0.97 $^{+0.06}_{-0.03}$
CS decays	A^{fac}	A^{pole}	B^{fac}	B^{pole}	$\mathcal{B}(10^{-4})$	α
$\Omega_c^0 \rightarrow \Sigma^+ K^-$	0	0.31	0	-0.32	0.52 $^{+1.22}_{-0.52}$	0.65(33)
$\Omega_c^0 \rightarrow \Sigma^0 K_{S/L}^0$	0	0.16	0	-0.16	0.13 $^{+0.31}_{-0.13}$	0.65(33)
$\Omega_c^0 \rightarrow \Xi^0 \pi^0$	0.44	2.54	-0.38	0.35	45.10(3.89)	0.01(1)
$\Omega_c^0 \rightarrow \Xi^0 \eta$	-0.92	-1.24	0.80	-1.24	21.35(5.63)	-0.13(4)
$\Omega_c^0 \rightarrow \Xi^- \pi^+$	-0.73	-3.59	0.64	-0.49	94.59(8.98)	0.02(1)
$\Omega_c^0 \rightarrow \Lambda K_{S/L}^0$	0	-1.99	0	0.78	18.74(1.96)	0.30(3)
DCS decays	A^{fac}	A^{pole}	B^{fac}	B^{pole}	$\mathcal{B}(10^{-5})$	α
$\Omega_c^0 \rightarrow \Sigma^+ \pi^-$	0	0.23	0	0.17	2.82(66)	-0.54(12)
$\Omega_c^0 \rightarrow \Sigma^0 \pi^0$	0	0.23	0	0.17	2.83(66)	-0.54(12)
$\Omega_c^0 \rightarrow \Sigma^- \pi^+$	0	0.23	0	0.17	2.82(66)	-0.54(12)
$\Omega_c^0 \rightarrow \Xi^- K^+$	-0.20	-0.50	0.18	0.08	23.11(1.84)	0.23(1)
$\Omega_c^0 \rightarrow p K^-$	0	0.26	0	0.13	3.24(1.13)	-0.43(7)
$\Omega_c^0 \rightarrow n K_{S/L}^0$	0	-0.18	0	-0.09	1.62(57)	-0.43(7)
$\Omega_c^0 \rightarrow \Lambda \eta$	0	-0.27	0	0.31	3.90(88)	0.76(10)

TABLE IV. Comparison with Ref. [35] for the CS decays of Ω_c^0 .

CS decays	This work		Current algebra [35]	
	$\mathcal{B}(10^{-4})$	α	$\mathcal{B}(10^{-4})$	α
$\Omega_c^0 \rightarrow \Sigma^+ K^-$	0.52 $^{+1.22}_{-0.52}$	0.65(33)	23.2	0.01
$\Omega_c^0 \rightarrow \Sigma^0 \bar{K}^0$	0.26 $^{+0.62}_{-0.26}$	0.65(33)	0.90	-0.03
$\Omega_c^0 \rightarrow \Xi^0 \pi^0$	45.10(3.89)	0.01(1)	54.6	0.04
$\Omega_c^0 \rightarrow \Xi^- \pi^+$	94.59(8.98)	0.02(1)	93.4	-0.03
$\Omega_c^0 \rightarrow \Lambda \bar{K}^0$	37.48(3.92)	0.30(3)	80.5	-0.01

TABLE V. Comparisons of the evaluated branching fractions with the experiments [1].

Channel	$\mathcal{C}'_+ = 1.20$	$\mathcal{C}'_+ = 1$	$\mathcal{C}'_+ = 0.469$	Data
$\mathcal{B}(\Omega_c^0 \rightarrow \Omega^- \pi^+)$	1.88(15)	1.30(10)	0.29(3)	...
$\mathcal{R}(\Omega_c^0 \rightarrow \Xi^0 K_S^0)$	0.12(4)	0.17(4)	0.76(25)	0.83(13)
$\mathcal{R}(\Omega_c^0 \rightarrow \Xi^- \pi^+)$	0.50(8)	0.73(13)	3.3(6)	0.253(60)
$\mathcal{R}(\Omega_c^0 \rightarrow \Xi^- K^+)$	0.012(2)	0.018(3)	0.080(15)	<0.07
$\mathcal{R}(\Omega_c^0 \rightarrow \Omega^- e^+ \nu_e)$	1.35	1.90	8.76	1.98(15)

with $\mathcal{B}(\Omega_c \rightarrow \mathbf{B}_n P)$ taken from Table III. We note that $\mathcal{C}'_+ = 1.2, 1$ and 0.469 come from the effective color scheme, $N_c = 3$ and $\mathbf{B}_c^A \rightarrow \mathbf{B}_n P$, respectively. The scheme of $\mathcal{C}'_+ = 0.469$ is favored by the experiment of $\mathcal{R}(\Omega_c^0 \rightarrow \Xi^0 K_S^0)$ but disfavored by the others. On the other hand, $\mathcal{R}(\Omega_c^0 \rightarrow \Omega^- e^+ \nu_e)$ suggests $\mathcal{C}'_+ = 1$. One shall

bear in mind that these outcomes are based on the LP scenario and the inconsistencies may disappear in the GP scenario which is not available due to a lack of experimental input.

C. Results of \mathbf{B}_{cc} decays

The CF decays of $\mathbf{B}_{cc} \rightarrow \mathbf{B}_c P$ based on the LP scenario are collected in Table VI, while the others in Appendix E. The lifetimes of the charmed baryons ($\Xi_{cc}^{++}, \Xi_{cc}^+, \Omega_{cc}^+$) are adopted as (256, 36, 136) fs, respectively. In analyzing the transition $\mathbf{B}_c^A \rightarrow \mathbf{B}_n P$, the fitted value of \mathcal{C}_+ is found to be notably smaller than the naïve expectation. This discrepancy prompts the consideration of two distinct cases: $\mathcal{C}_+ = 0.469$ and $\mathcal{C}_+ = 1$. All other parameters in this analysis are from Eq. (56).

The branching ratio of $\mathcal{R}_{\Xi_{cc}} = \mathcal{B}(\Xi_{cc}^{++} \rightarrow \Xi_c^+ \pi^+) / \mathcal{B}(\Xi_{cc}^{++} \rightarrow \Xi_c^+ \pi^+)$ is calculated to be 1.19 ± 0.09 and 0.87 ± 0.06 for $\mathcal{C}_+ = 0.469$ and 1, respectively. These results are roughly consistent with the experimental measurement of $1.41 \pm 0.17 \pm 0.10$ [72]. As $\mathcal{R}_{\Xi_{cc}}$ is not included in the global fit, it is nontrivial for our outcome to agree with the experiment. Nevertheless, the calculated branching fraction $\mathcal{B}(\Xi_{cc} \rightarrow \Xi_c^+ \pi^+) = (6.24 \pm 0.21)\%$ with $\mathcal{C}_+ = 1$ exceeds the naïve expectation of $(1.33 \pm 0.74)\%$, referenced in [73, 74]. The comparison with the soft-meson limit [73] for CF decays is given in Table VII. We see that our predictions for the branching fractions are systematically smaller than those in Ref. [73]

TABLE VI. Predictions of the CF decays in $\mathbf{B}_{cc} \rightarrow \mathbf{B}_c^{A,S}P$ with $\mathcal{C}_+ = 0.469$ and 1, where A and B are in units of $10^{-2}G_F \text{ GeV}^2$.

Channels	Results with $\mathcal{C}_+ = 0.469$					Results with $\mathcal{C}_+ = 1$		
	A^{fac}	A^{pole}	B^{fac}	B^{pole}	$\mathcal{B}(\%)$	α	$\mathcal{B}(\%)$	α
$\Xi_{cc}^{++} \rightarrow \Xi_c^+ \pi^+$	5.36	-1.22	7.59	-5.43	0.99(21)	-0.19(7)	6.24(21)	-0.38(7)
$\Xi_{cc}^{++} \rightarrow \Sigma_c^{++} K_S$	-3.29	0	-22.12	0	1.34(13)	-0.99(0)	1.34(13)	-0.99(0)
$\Xi_{cc}^{++} \rightarrow \Sigma_c^{++} K_L$	2.96	0	19.89	0	1.08(11)	-0.99(0)	1.08(11)	-0.99(0)
$\Xi_{cc}^{++} \rightarrow \Xi_c^{\prime+} \pi^+$	-2.80	0	-22.31	0	1.18(18)	-0.96(0)	5.41(18)	-0.96(0)
$\Xi_{cc}^+ \rightarrow \Xi_c^0 \pi^+$	-5.34	-5.74	-7.60	0	1.00(9)	-0.25(1)	2.44(9)	-0.34(1)
$\Xi_{cc}^+ \rightarrow \Xi_c^+ \pi^0$	0	4.92	0	3.84	0.20(3)	-0.29(4)	0.20(3)	-0.29(4)
$\Xi_{cc}^+ \rightarrow \Xi_c^+ \eta$	0	-2.37	0	-1.85	0.04(1)	-0.26(3)	0.04(1)	-0.26(3)
$\Xi_{cc}^+ \rightarrow \Lambda_c^+ K_S$	4.61	3.34	5.27	-0.17	0.51(2)	-0.26(0)	0.51(2)	-0.26(0)
$\Xi_{cc}^+ \rightarrow \Lambda_c^+ K_L$	-4.15	-3.42	-4.74	-0.17	0.46(2)	-0.27(1)	0.46(2)	-0.27(1)
$\Xi_{cc}^+ \rightarrow \Sigma_c^{++} K^-$	0	1.87	0	0	0.03(1)	0(0)	0.03(1)	0(0)
$\Xi_{cc}^+ \rightarrow \Sigma_c^+ K_S$	-2.33	-0.93	-15.64	0	0.13(1)	-0.98(1)	0.13(1)	-0.98(1)
$\Xi_{cc}^+ \rightarrow \Sigma_c^+ K_L$	2.09	0.93	14.07	0	0.11(1)	-0.98(1)	0.11(1)	-0.98(1)
$\Xi_{cc}^+ \rightarrow \Xi_c^{\prime+} \pi^0$	0	-1.12	0	0	0.01(0)	0(0)	0.01(0)	0(0)
$\Xi_{cc}^+ \rightarrow \Xi_c^{\prime+} \eta$	0	-1.62	0	0	0.02(0)	0(0)	0.02(0)	0(0)
$\Xi_{cc}^+ \rightarrow \Xi_c^{\prime0} \pi^+$	-2.80	-1.59	-22.31	0	0.25(4)	-0.99(0)	0.92(4)	-1.00(0)
$\Xi_{cc}^+ \rightarrow \Omega_c^0 K^+$	0	-1.87	0	0	0.02(1)	0(0)	0.02(1)	0(0)
$\Omega_{cc}^+ \rightarrow \Xi_c^+ K_S$	-4.53	0.54	-5.57	3.20	0.49(6)	-0.23(4)	0.49(6)	-0.23(4)
$\Omega_{cc}^+ \rightarrow \Xi_c^+ K_L$	4.08	-0.90	5.01	-3.20	0.31(4)	-0.22(5)	0.31(4)	-0.22(5)
$\Omega_{cc}^+ \rightarrow \Xi_c^{\prime+} K_S$	-2.40	-0.05	-16.36	0	0.40(0)	-0.99(0)	0.40(0)	-0.99(0)
$\Omega_{cc}^+ \rightarrow \Xi_c^{\prime+} K_L$	2.16	-0.05	14.72	0	0.31(0)	-0.98(0)	0.31(0)	-0.98(0)
$\Omega_{cc}^+ \rightarrow \Omega_c^0 \pi^+$	-4.11	0	-32.96	0	1.41(21)	-0.96(0)	6.47(21)	-0.96(0)

TABLE VII. Comparison with Ref. [73] for the CF decays of \mathbf{B}_{cc} .

Channels	This work		Current algebra [73]	
	$\mathcal{B}(\%)$	α	$\mathcal{B}(\%)$	α
$\Xi_{cc}^+ \rightarrow \Xi_c^0 \pi^+$	1.00(9)	-0.25(1)	3.84	-0.31
$\Xi_{cc}^+ \rightarrow \Xi_c^{\prime0} \pi^+$	0.25(4)	-0.99(0)	1.55	-0.73
$\Xi_{cc}^+ \rightarrow \Xi_c^+ \pi^0$	0.20(3)	-0.30(4)	2.38	-0.25
$\Xi_{cc}^+ \rightarrow \Xi_c^{\prime+} \pi^0$	0.01(0)	0(0)	0.17	-0.03
$\Xi_{cc}^+ \rightarrow \Sigma_c^{++} K^-$	0.03(1)	0(0)	0.13	0.04
$\Xi_{cc}^+ \rightarrow \Omega_c^0 K^+$	0.02(1)	0(0)	0.06	-0.03
$\Omega_{cc}^+ \rightarrow \Omega_c^0 \pi^+$	1.41(21)	-0.96(0)	3.96	-0.83

by an order of magnitude, although we agree well in terms of α .

Note that $\Xi_{cc}^{++} \rightarrow \Sigma_{cc}^{++} K_{S/L}$ do not receive pole contributions, and the ratio

$$\frac{\mathcal{B}(\Xi_{cc}^{++} \rightarrow \Sigma_{cc}^{++} K_S^0) - \mathcal{B}(\Xi_{cc}^{++} \rightarrow \Sigma_{cc}^{++} K_L^0)}{\mathcal{B}(\Xi_{cc}^{++} \rightarrow \Sigma_{cc}^{++} K_S^0) + \mathcal{B}(\Xi_{cc}^{++} \rightarrow \Sigma_{cc}^{++} K_L^0)} = \frac{2s_c^2}{1 + s_c^4} \approx 10\% \quad (61)$$

serves as an important prediction of the pole approximation. We emphasize that the differences between two cases only occur in A^{fac} and B^{fac} with charged P , related by a factor of $1/0.469$.

Due to the smallness of the Ξ_{cc}^+ lifetime, the branching fractions of Ξ_{cc}^+ are systematically smaller, but the predicted $\mathcal{B}(\Xi_{cc}^+ \rightarrow \Xi_c^0 \pi^+)$ is still huge. Particularly, with $\mathcal{C}_+ = 1$, we find $\mathcal{B}(\Xi_{cc}^+ \rightarrow \Xi_c^0 \pi^+ \rightarrow \Xi^- \pi^+ \pi^+ \pi^+ \pi^-) = (1.1 \pm 0.6) \times 10^{-3}$, where $\mathcal{B}(\Xi_c^0 \rightarrow \Xi^- \pi^+ \pi^+ \pi^-) = (4.8 \pm 2.3)\%$ is used [1]. As the final state particles are all charged, searches of $\Xi_{cc}^+ \rightarrow \Xi^- \pi^+ \pi^+ \pi^+ \pi^-$ are recommended. In addition $\mathcal{B}(\Omega_{cc}^+ \rightarrow \Omega_c^0 \pi^+)$ consists solely of factorizable contributions and is predicted to be notably large. It is also recommended for future experimental investigations.

Finally, it is important to note that the LP scenario functions as an initial estimation in the decays of doubly charmed baryons. Although consistency have been observed in $\mathcal{R}_{\Xi_{cc}^+}$, for more robust and reliable results, it is advisable to refer to the GP scenario when more experimental data becomes available.

VI. SUMMARY

We have analyzed the two-body nonleptonic weak decays of charmed baryons using the pole approximation in conjunction with the $SU(3)_F$ symmetry. We have shown that the KPW theorem demands that $O_+^{qq'}$ and P form a **3** representation in the $SU(3)_F$ group, reducing the numbers of the free parameters significantly. In particular, Eqs. (25)–(27) are given for the first time. With the GP scenario, most of the experimental data of $\mathbf{B}_c^A \rightarrow \mathbf{B}_n P$ can be explained, but inconsistencies with the experiments have been found

in $\alpha(\Lambda_c^+ \rightarrow pK_S^0)$, $\mathcal{B}(\Xi_c^0 \rightarrow \Xi^- \pi^+)$ and $\mathcal{B}(\Xi_c^0 \rightarrow \Xi^- K^+)$. These inconsistencies are recommended to be revisited in future experiments.

Furthermore, by assuming the dominance of the low-lying intermediate baryons, we have obtained the ability to make several predictions for $\Omega_c^0 \rightarrow \mathbf{B}_n P$ and $\mathbf{B}_{cc} \rightarrow \mathbf{B}_c^{A,S} P$ based on the experimental input of $\mathbf{B}_c^A \rightarrow \mathbf{B}_n P$. The fitted value $\mathcal{C}_+ = 0.469$ is significantly smaller than the naïve expectation of $\mathcal{C}_+ \approx 1$. In addition the LP scenario fails to explain $\mathcal{B}_{\text{exp}}(\Lambda_c^+ \rightarrow \Xi^0 K^+)$ and $\mathcal{B}_{\text{exp}}(\Lambda_c \rightarrow n\pi^+)$ though consistencies have been found with the soft-meson limit [38]. To search for the evidence of Ξ_{cc}^+ , we have recommended the decay channel of $\Xi_{cc}^+ \rightarrow \Xi_c^0 \pi^+ \rightarrow \Xi^- \pi^+ \pi^+ \pi^-$, of which the branching fraction is found to be $(1.1 \pm 0.6) \times 10^{-3}$. The predictions for the nonleptonic weak decay channels have been collected in Appendix E, to be used as a reference for future experiments seeking verification.

ACKNOWLEDGMENTS

The author extends gratitude to Hai-Yang Cheng for the insightful discussions. This research was supported by the National Natural Science Foundation of China under Grant No. 12205063.

APPENDIX A: ROLE OF SPECTATOR QUARKS

In this appendix, we discuss few types of quark models where spectator quarks affect little to the baryon matrix elements.

In the MIT bag model, for $|\vec{x}| < R$ the bag quark wave functions are [75]

$$\phi_{q\uparrow}^a(\vec{x}) = N_q \begin{pmatrix} \omega_q^+ j_0(p_q r) \chi_\uparrow \\ i\omega_q^- j_1(p_q r) \hat{x} \cdot \vec{\sigma} \chi_\uparrow \end{pmatrix}_a, \quad (\text{A1})$$

whereas $\phi(\vec{x}) = 0$ for $|\vec{x}| > R$ with R the bag radius. In Eq. (A1), $\chi_\uparrow = (1, 0)^T$ and $\chi_\downarrow = (0, 1)^T$ denote the states with $J_z = \pm 1/2$. The functions $j_{0,1}$ represent the spherical Bessel functions, and the kinetic factors are defined as $\omega_q^\pm = \sqrt{E_q \pm m_q}$ with E_q and m_q the quark energy and mass. The normalization factor of N_q is determined by the normalization condition $\int d^3x \phi_q^\dagger(\vec{x}) \phi_q(\vec{x}) = 1$.

The baryon wave function is made of a direct product of three bag quarks

$$\Psi(\vec{x}_1, \vec{x}_2, \vec{x}_3) = \phi_{q_1}(\vec{x}_1) \phi_{q_2}(\vec{x}_2) \phi_{q_3}(\vec{x}_3). \quad (\text{A2})$$

To examine the effects of the spectator quarks, we do not write down the spinor indices which are irrelevant to the argument. Taking $c \rightarrow s$ transition at quark level for instance, we have that

$$\begin{aligned} \langle \mathcal{B}_f | s^\dagger \Upsilon c | \mathcal{B}_i \rangle &= \int d^3x_1 d^3x_2 d^3x_3 (\phi_s^\dagger(\vec{x}_3) \Upsilon \phi_c(\vec{x}_3)) \\ &\quad \times \sum_{j=1,2} \phi_{q_j}^\dagger(\vec{x}_j) \phi_{q_j}(\vec{x}_j) \\ &= \int d^3x_3 (\phi_s^\dagger(\vec{x}_3) \Upsilon \phi_c(\vec{x}_3)), \end{aligned} \quad (\text{A3})$$

where Υ is an arbitrary 4×4 Dirac matrix and we have used $\int d^3x \phi_q^\dagger(\vec{x}) \phi_q(\vec{x}) = 1$ in the second line. Given the distinct behaviors of ϕ_c and ϕ_s , the $SU(4)_F$ symmetry is significantly broken. However, as Eq. (A3) is not influenced by the spectator quarks, there exists a relationship between $\Lambda_c^+ \rightarrow \Lambda$ and $\Xi_{cc}^{++} \rightarrow \Xi_c^+$, modulated by a spin-flavor factor. In other words, while the matrix elements maintain invariance when interchanging $d \leftrightarrow c$ for the spectator quark, they do not uphold this invariance for the transited quark. This characteristic arises because the quark states in Eq. (A2) are untangled, allowing the spectator quarks to be integrated out independently during the weak interaction. It is straightforward to show that the statement also holds for the four-quark operator matrix elements.⁴

This property serves as an excellent approximation even when considering more sophisticated scenarios. In the homogeneous bag model (HBM), the bag wave functions are entangled and Eq. (A2) is modified as [74]

$$\begin{aligned} \Psi(\vec{x}_1, \vec{x}_2, \vec{x}_3) &= \int d^3x_\Delta \phi_{q_1}(\vec{x}_1 - \vec{x}_\Delta) \phi_{q_2}(\vec{x}_2 - \vec{x}_\Delta) \\ &\quad \times \phi_{q_3}(\vec{x}_3 - \vec{x}_\Delta). \end{aligned} \quad (\text{A4})$$

Here, the integration of \vec{x}_Δ causes the spatial distributions of (q_1, q_2, q_3) to become entangled and Eq. (A3) is adjusted as follows:

$$\begin{aligned} \langle \mathcal{B}_f | s^\dagger \Upsilon c | \mathcal{B}_i \rangle &= \int d^3x_3 d^3x_\Delta \phi_s^\dagger\left(\vec{x}_3 + \frac{1}{2}\vec{x}_\Delta\right) \\ &\quad \times \Upsilon \phi_c\left(\vec{x}_3 - \frac{1}{2}\vec{x}_\Delta\right) \sum_{j=1,2} \mathcal{D}_{q_j}(\vec{x}_\Delta), \end{aligned} \quad (\text{A5})$$

with

$$\mathcal{D}_{q_j}(\vec{x}_\Delta) = \int d^3x \phi_q^\dagger\left(\vec{x}_1 + \frac{1}{2}\vec{x}_\Delta\right) \phi_q\left(\vec{x}_1 - \frac{1}{2}\vec{x}_\Delta\right). \quad (\text{A6})$$

Here, $\phi_s^\dagger \Upsilon \phi_c$ describes the $c \rightarrow s$ transition, and \mathcal{D}_{q_j} is the overlap of the spectator quarks between \mathcal{B}_i and \mathcal{B}_f . As the positions of quarks in a baryon are now correlated, we see

⁴The relations among doubly and singly charmed baryon transitions can be seen explicitly by comparing Refs. [38] with [73]. For instance, from Eq. (31) in Ref. [73] and Eq. (D2) in Ref. [38] we find $-2\langle \Sigma^+ | O_- | \Lambda_c^+ \rangle = \langle \Xi_c^+ | O_- | \Xi_{cc}^+ \rangle$, which can be derived also from Eq. (44) in this work.

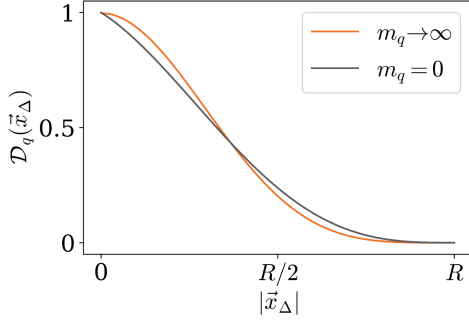


FIG. 4. The weight function of $\mathcal{D}_q(\vec{x}_\Delta)$ at the limits of $m_q = 0$ and $m_q \rightarrow \infty$.

that the spectator quarks affect the matrix elements in Eq. (A5) as a weight function to the quark transition of $c \rightarrow s$. It turns out that \mathcal{D}_q depends little on the quark mass as it is related to the normalization [$\mathcal{D}_q(0) = 1$]. In Fig. 4, we plot the \vec{x}_Δ dependency of \mathcal{D}_q with $m_q = 0$ and $m_q \rightarrow \infty$. In the figure, the difference between the two lines is less than 7%, which is lower than the $SU(3)_F$ symmetry breaking effects.

Finally, we use the nonrelativistic constituent quark model (NRQM) as our last example. Define

$$\langle O_1^u \rangle_B = \langle B | [\bar{c}\gamma^\mu(1 - \gamma_5)u][\bar{u}\gamma_\mu(1 - \gamma_5)c] | B \rangle$$

with the normalization of $\bar{u}_B u_B = 1$. Assuming that the spectator quark has minimal impact, from Eq. (44) we deduce

$$\langle O_1^u \rangle_{\Xi_c^+} = 6 \langle O_1^u \rangle_{\Xi_c^{++}}. \quad (\text{A7})$$

The actual calculations yield $\langle O_1^u \rangle_{\Xi_c^+} = 0.54 \pm 0.16$ [22] and $\langle O_1^u \rangle_{\Xi_c^{++}} = 4.0 \pm 1.0$ [23] in units of 10^{-2} GeV^3 , which are consistent with Eq. (A7) within the uncertainties.

Similar results are also observed for other charmed baryons.

In conclusion, the assumption on the spectator quark is exact in the MIT bag model and empirically substantiated in both HBM and NRQM.

APPENDIX B: EFFECTIVE COLOR NUMBER

The decay of $\Lambda_c^+ \rightarrow p\phi$ does not receive the W -exchange contributions. From LQCD, the decay constant of ϕ is found to be $f_\phi = 0.241(9) \text{ GeV}$ [76] and the form factors of $\Lambda_c^+ \rightarrow p$ are [66]

$$(f_1, f_2, g_1, g_2) = (0.939, 0.524, 0.785, -0.050), \quad (\text{B1})$$

at $q^2 = M_p^2$. Combing with $\mathcal{B}_{\text{exp}}(\Lambda_c \rightarrow p\phi) = (1.06 \pm 0.14) \times 10^{-3}$, we find

$$\mathcal{C}_0 = c_2 + \frac{c_1}{N_c^{\text{eff}}} = -0.36 \pm 0.04, \quad (\text{B2})$$

where N_c^{eff} is the effective color number. The formalism of the decay width and the definitions of $f_{1,2}$ and $g_{1,2}$ can be found in Ref. [38]. In the effective color number approach, one assume $\mathcal{C}_+ = c_1 + c_2/N_c^{\text{eff}}$ with N_c^{eff} fitted by Eq. (B2). The values of \mathcal{C}_+ at different energy scales are collected in Table VIII, where the naive expectations with $N_c^{\text{eff}} = N_c = 3$ are also listed.

In the naive factorization approach, though \mathcal{C}_+ behaves stably, \mathcal{C}_0 varies heavily according to the energy scale and flip sign at the next-to-leading order (NLO). It is a sign that the naive factorization approach cannot be trusted. On the other hand, the effective color approach provides a much stable value of \mathcal{C}_+ .

TABLE VIII. The effective Wilson coefficient, where $\mathcal{C}_+(N_c^{\text{eff}})$ is fitted from Eq. (B2). The values of $c_{1,2}$ are from Ref. [63].

	μ [GeV]	c_1	c_2	$\mathcal{C}_+(N_c^{\text{eff}})$	$\mathcal{C}_+(N_c = 3)$	$\mathcal{C}_0(N_c = 3)$
LO	1.0	1.422	-0.742	1.23 ± 0.01	1.175	-0.268
	1.5	1.298	-0.565	1.22 ± 0.01	1.110	-0.132
	2.0	1.239	-0.475	1.20 ± 0.01	1.081	-0.062
NLO	1.0	1.275	-0.510	1.22 ± 0.01	1.105	-0.085
	1.5	1.188	-0.378	1.19 ± 0.01	1.062	0.018
	2.0	1.148	-0.311	1.17 ± 0.01	1.044	0.072

APPENDIX C: PARAMETRIZATION IN THE LP SCENARIO

In this section, we assemble the parametrizations under the LP scenario. Tables IX–XI encompass the expressions for CF, CS, and DCS decay modes of \mathbf{B}_c^A decays. The expressions for Ω_c^0 decays are consolidated in Table XII. Furthermore, Tables XIII–XV include the expressions for CF, CS, and DCS decay modes of \mathbf{B}_{cc} decays.

TABLE IX. The parametrizations of A^{fac} and A^{pole} in the LP scenario for the CF decays of $\mathbf{B}_c^{A,S} \rightarrow \mathbf{B}_n P$. In the global fit, we absorb g'_1 into \tilde{b} and \tilde{b}' by redefinition. The ones of B^{fac} and B^{pole} can be obtained by the substitutions in Eqs. (49) and (53).

Channels	$\frac{\sqrt{2}}{G_F V_{cs}^* V_{ud} f_P} A^{\text{fac}}$	$\frac{f_P}{\sqrt{2}} A^{\text{pole}}$
$\Lambda_c^+ \rightarrow \Lambda^0 \pi^+$	$-\frac{C_+(A_1+A_2)}{6}$	$\frac{(g'_1-2g'_2)(-R_c^{As} \tilde{b}-R_c^{Au}(\mathbf{6})\tilde{b}')}{3}$
$\Lambda_c^+ \rightarrow \Sigma^+ \pi^0$	0	$\frac{\sqrt{3}(R_c^{As} \tilde{b}g'_1-R_c^{Au}(\mathbf{6})\tilde{b}'(g'_1-2g'_2))}{3}$
$\Lambda_c^+ \rightarrow \Sigma^+ \eta$	0	$-\frac{R_c^{As} \tilde{b}(g'_1-2g'_2)}{3} + \frac{R_c^{Au}(\mathbf{3})\tilde{b}'(5g'_1-4g'_2)}{9}$
$\Lambda_c^+ \rightarrow \Sigma^0 \pi^+$	0	$\frac{\sqrt{3}(-R_c^{As} \tilde{b}g'_1+R_c^{Au}(\mathbf{6})\tilde{b}'(g'_1-2g'_2))}{3}$
$\Lambda_c^+ \rightarrow \Xi^0 K^+$	0	$\frac{\sqrt{6}(6R_c^{As} \tilde{b}g'_2+R_c^{Au}(\mathbf{3})\tilde{b}'(5g'_1-4g'_2)-3R_c^{Au}(\mathbf{6})\tilde{b}'(g'_1-2g'_2))}{18}$
$\Lambda_c^+ \rightarrow p K_L$	$\frac{\sqrt{3}C_0(-A_1s_c^2+A_1-A_2s_c^2+A_2)}{12}$	$\frac{\sqrt{3}(-6R_c^{As} \tilde{b}(g'_1-g'_2)+R_c^{Au}(\mathbf{3})\tilde{b}'s_c^2(5g'_1-4g'_2)+3R_c^{Au}(\mathbf{6})\tilde{b}'s_c^2(g'_1-2g'_2))}{18}$
$\Lambda_c^+ \rightarrow p K_S$	$-\frac{\sqrt{3}C_0(A_1s_c^2+A_1+A_2s_c^2+A_2)}{12}$	$\frac{\sqrt{3}(6R_c^{As} \tilde{b}(g'_1-g'_2)+R_c^{Au}(\mathbf{3})\tilde{b}'s_c^2(5g'_1-4g'_2)+3R_c^{Au}(\mathbf{6})\tilde{b}'s_c^2(g'_1-2g'_2))}{18}$
$\Xi_c^+ \rightarrow \Sigma^+ K_L$	$\frac{\sqrt{3}C_0(-A_1s_c^2+A_1-A_2s_c^2+A_2)}{12}$	$\frac{\sqrt{3}(6R_c^{As} \tilde{b}s_c^2(g'_1-g'_2)-R_c^{Au}(\mathbf{3})\tilde{b}'(5g'_1-4g'_2)-3R_c^{Au}(\mathbf{6})\tilde{b}'(g'_1-2g'_2))}{18}$
$\Xi_c^+ \rightarrow \Sigma^+ K_S$	$-\frac{\sqrt{3}C_0(A_1s_c^2+A_1+A_2s_c^2+A_2)}{12}$	$\frac{\sqrt{3}(6R_c^{As} \tilde{b}s_c^2(g'_1-g'_2)+R_c^{Au}(\mathbf{3})\tilde{b}'(5g'_1-4g'_2)+3R_c^{Au}(\mathbf{6})\tilde{b}'(g'_1-2g'_2))}{18}$
$\Xi_c^+ \rightarrow \Xi^0 \pi^+$	$\frac{\sqrt{6}C_+(A_1+A_2)}{12}$	$\frac{\sqrt{6}\tilde{b}'(R_c^{Au}(\mathbf{3})(5g'_1-4g'_2)+3R_c^{Au}(\mathbf{6})(g'_1-2g'_2))}{18}$
$\Xi_c^0 \rightarrow \Lambda^0 K_L$	$\frac{\sqrt{2}C_0(-A_1s_c^2+A_1-A_2s_c^2+A_2)}{24}$	$\frac{\sqrt{2}(-R_c^{As} \tilde{b}s_c^2(g'_1+g'_2)-R_c^{As} \tilde{b}(2g'_1-g'_2)+2R_c^{Au}(\mathbf{6})\tilde{b}'s_c^2(g'_1-2g'_2)+R_c^{Au}(\mathbf{6})\tilde{b}'(g'_1-2g'_2))}{6}$
$\Xi_c^0 \rightarrow \Lambda^0 K_S$	$-\frac{\sqrt{2}C_0(A_1s_c^2+A_1+A_2s_c^2+A_2)}{24}$	$\frac{\sqrt{2}(-R_c^{As} \tilde{b}s_c^2(g'_1+g'_2)+R_c^{As} \tilde{b}(2g'_1-g'_2)+2R_c^{Au}(\mathbf{6})\tilde{b}'s_c^2(g'_1-2g'_2)-R_c^{Au}(\mathbf{6})\tilde{b}'(g'_1-2g'_2))}{6}$
$\Xi_c^0 \rightarrow \Sigma^+ K^-$	0	$\frac{\sqrt{6}(-6R_c^{As} \tilde{b}g'_2-R_c^{Au}(\mathbf{3})\tilde{b}'(5g'_1-4g'_2)+3R_c^{Au}(\mathbf{6})\tilde{b}'(g'_1-2g'_2))}{18}$
$\Xi_c^0 \rightarrow \Sigma^0 K_L$	$\frac{\sqrt{6}C_0(-A_1s_c^2+A_1-A_2s_c^2+A_2)}{24}$	$\frac{\sqrt{6}(R_c^{As} \tilde{b}g'_2+R_c^{As} \tilde{b}s_c^2(g'_1-g'_2)-R_c^{Au}(\mathbf{6})\tilde{b}'(g'_1-2g'_2))}{6}$
$\Xi_c^0 \rightarrow \Sigma^0 K_S$	$-\frac{\sqrt{6}C_0(A_1s_c^2+A_1+A_2s_c^2+A_2)}{24}$	$\frac{\sqrt{6}(-R_c^{As} \tilde{b}g'_2+R_c^{As} \tilde{b}s_c^2(g'_1-g'_2)+R_c^{Au}(\mathbf{6})\tilde{b}'(g'_1-2g'_2))}{6}$
$\Xi_c^0 \rightarrow \Xi^0 \pi^0$	0	$\frac{\sqrt{3}(-6R_c^{As} \tilde{b}(g'_1-g'_2)+R_c^{Au}(\mathbf{3})\tilde{b}'(5g'_1-4g'_2)+3R_c^{Au}(\mathbf{6})\tilde{b}'(g'_1-2g'_2))}{18}$
$\Xi_c^0 \rightarrow \Xi^0 \eta$	0	$\frac{R_c^{As} \tilde{b}(g'_1+g'_2)}{3} + \frac{R_c^{Au}(\mathbf{3})\tilde{b}'(5g'_1-4g'_2)}{18} - \frac{R_c^{Au}(\mathbf{6})\tilde{b}'(g'_1-2g'_2)}{2}$
$\Xi_c^0 \rightarrow \Xi^- \pi^+$	$\frac{\sqrt{6}C_+(A_1+A_2)}{12}$	$\frac{\sqrt{6}R_c^{As} \tilde{b}(g'_1-g'_2)}{3}$

TABLE X. The legend is identical to that of Table IX but for CS decays.

Channels	$\frac{\sqrt{2}}{G_F V_{cs}^* V_{ud} s_c f_P} A^{\text{fac}}$	$\frac{f_P}{\sqrt{2} s_c} A^{\text{pole}}$
$\Lambda_c^+ \rightarrow \Lambda^0 K^+$	$-\frac{s_c C_+(A_1+A_2)}{6}$	$\frac{s_c(-2R_c^{As} \tilde{b}(g'_1+g'_2)-R_c^{Au}(\mathbf{3})\tilde{b}'(5g'_1-4g'_2)+R_c^{Au}(\mathbf{6})\tilde{b}'(g'_1-2g'_2))}{6}$
$\Lambda_c^+ \rightarrow \Sigma^+ K_{S/L}$	0	$\frac{\sqrt{3}s_c(-6R_c^{As} \tilde{b}(g'_1-g'_2)+R_c^{Au}(\mathbf{3})\tilde{b}'(5g'_1-4g'_2)+3R_c^{Au}(\mathbf{6})\tilde{b}'(g'_1-2g'_2))}{18}$
$\Lambda_c^+ \rightarrow \Sigma^0 K^+$	0	$\frac{\sqrt{3}s_c(-6R_c^{As} \tilde{b}(g'_1-g'_2)+R_c^{Au}(\mathbf{3})\tilde{b}'(5g'_1-4g'_2)+3R_c^{Au}(\mathbf{6})\tilde{b}'(g'_1-2g'_2))}{18}$
$\Lambda_c^+ \rightarrow p \pi^0$	$\frac{\sqrt{3}s_c C_0(A_1+A_2)}{12}$	$\frac{\sqrt{3}s_c(R_c^{As} \tilde{b}g'_2-R_c^{Au}(\mathbf{6})\tilde{b}'(g'_1-2g'_2))}{3}$
$\Lambda_c^+ \rightarrow p \eta$	$-\frac{s_c C_0(A_1+A_2)}{4}$	$\frac{s_c(3R_c^{As} \tilde{b}(2g'_1-g'_2)+R_c^{Au}(\mathbf{3})\tilde{b}'(5g'_1-4g'_2))}{9}$
$\Lambda_c^+ \rightarrow n \pi^+$	$-\frac{\sqrt{6}s_c C_+(A_1+A_2)}{12}$	$\frac{\sqrt{6}s_c(R_c^{As} \tilde{b}g'_2-R_c^{Au}(\mathbf{6})\tilde{b}'(g'_1-2g'_2))}{3}$
$\Xi_c^+ \rightarrow \Lambda^0 \pi^+$	$-\frac{s_c C_+(A_1+A_2)}{12}$	$\frac{s_c(2R_c^{As} \tilde{b}(g'_1-2g'_2)-R_c^{Au}(\mathbf{3})\tilde{b}'(5g'_1-4g'_2)-R_c^{Au}(\mathbf{6})\tilde{b}'(g'_1-2g'_2))}{6}$
$\Xi_c^+ \rightarrow \Sigma^+ \pi^0$	$\frac{\sqrt{3}s_c C_0(A_1+A_2)}{12}$	$\frac{\sqrt{3}s_c(-6R_c^{As} \tilde{b}g'_1-R_c^{Au}(\mathbf{3})\tilde{b}'(5g'_1-4g'_2)+3R_c^{Au}(\mathbf{6})\tilde{b}'(g'_1-2g'_2))}{18}$
$\Xi_c^+ \rightarrow \Sigma^+ \eta$	$-\frac{s_c C_+(A_1+A_2)}{4}$	$\frac{s_c(6R_c^{As} \tilde{b}(g'_1-2g'_2)+R_c^{Au}(\mathbf{3})\tilde{b}'(5g'_1-4g'_2)+9R_c^{Au}(\mathbf{6})\tilde{b}'(g'_1-2g'_2))}{18}$

(Table continued)

TABLE X. (Continued)

Channels	$\frac{\sqrt{2}}{G_F} \frac{1}{V_{cs}^* V_{ud} s_c^2} A^{\text{fac}}$	$\frac{f_P}{\sqrt{2} s_c} A^{\text{pole}}$
$\Xi_c^+ \rightarrow \Sigma^0 \pi^+$	$\frac{\sqrt{3} s_c C_+(A_1+A_2)}{12}$	$\frac{\sqrt{3} s_c (6R_c^{As} \bar{b} g_1' + R_c^{Au} (\bar{3}) \bar{b}' (5g_1' - 4g_2') - 3R_c^{Au} (\bar{6}) \bar{b}' (g_1' - 2g_2'))}{18}$
$\Xi_c^+ \rightarrow \Xi^0 K^+$	$\frac{\sqrt{6} s_c C_+(A_1+A_2)}{12}$	$\frac{\sqrt{6} s_c (-R_c^{As} \bar{b} g_1' + R_c^{Au} (\bar{6}) \bar{b}' (g_1' - 2g_2'))}{3}$
$\Xi_c^+ \rightarrow p K_{S/L}$	0	$\frac{\sqrt{3} s_c (6R_c^{As} \bar{b} (g_1' - g_2') - R_c^{Au} (\bar{3}) \bar{b}' (5g_1' - 4g_2') - 3R_c^{Au} (\bar{6}) \bar{b}' (g_1' - 2g_2'))}{18}$
$\Xi_c^0 \rightarrow \Lambda^0 \pi^0$	$\frac{\sqrt{2} s_c C_0(A_1+A_2)}{24}$	$\frac{\sqrt{2} s_c (2R_c^{As} \bar{b} (g_1' - 2g_2') - R_c^{Au} (\bar{3}) \bar{b}' (5g_1' - 4g_2') - R_c^{Au} (\bar{6}) \bar{b}' (g_1' - 2g_2'))}{12}$
$\Xi_c^0 \rightarrow \Lambda^0 \eta$	$-\frac{\sqrt{6} s_c C_0(A_1+A_2)}{24}$	$\frac{\sqrt{6} s_c (6R_c^{As} \bar{b} (g_1' - 2g_2') - R_c^{Au} (\bar{3}) \bar{b}' (5g_1' - 4g_2') + 3R_c^{Au} (\bar{6}) \bar{b}' (g_1' - 2g_2'))}{36}$
$\Xi_c^0 \rightarrow \Sigma^+ \pi^-$	0	$\frac{\sqrt{6} s_c (6R_c^{As} \bar{b} g_2' + 5R_c^{Au} (\bar{3}) \bar{b}' g_1' - 4R_c^{Au} (\bar{3}) \bar{b}' g_2' - 3R_c^{Au} (\bar{6}) \bar{b}' g_1' + 6R_c^{Au} (\bar{6}) \bar{b}' g_2')}{18}$
$\Xi_c^0 \rightarrow \Sigma^0 \pi^0$	$\frac{\sqrt{6} s_c C_0(A_1+A_2)}{24}$	$\frac{\sqrt{6} s_c (-6R_c^{As} \bar{b} (g_1' - 2g_2') + R_c^{Au} (\bar{3}) \bar{b}' (5g_1' - 4g_2') - 3R_c^{Au} (\bar{6}) \bar{b}' (g_1' - 2g_2'))}{36}$
$\Xi_c^0 \rightarrow \Sigma^0 \eta$	$-\frac{\sqrt{2} s_c C_0(A_1+A_2)}{8}$	$\frac{\sqrt{2} s_c (6R_c^{As} \bar{b} (g_1' - 2g_2') + R_c^{Au} (\bar{3}) \bar{b}' (5g_1' - 4g_2') + 9R_c^{Au} (\bar{6}) \bar{b}' (g_1' - 2g_2'))}{36}$
$\Xi_c^0 \rightarrow \Sigma^- \pi^+$	$-\frac{\sqrt{6} s_c C_+(A_1+A_2)}{12}$	$\frac{\sqrt{6} R_c^{As} \bar{b} s_c (-g_1' + g_2')}{3}$
$\Xi_c^0 \rightarrow \Xi^0 K_{S/L}$	0	$\frac{\sqrt{3} s_c (R_c^{As} \bar{b} g_1' - R_c^{Au} (\bar{6}) \bar{b}' g_1' + 2R_c^{Au} (\bar{6}) \bar{b}' g_2')}{3}$
$\Xi_c^0 \rightarrow \Xi^- K^+$	$\frac{\sqrt{6} s_c C_+(A_1+A_2)}{12}$	$\frac{\sqrt{6} R_c^{As} \bar{b} s_c (g_1' - g_2')}{3}$
$\Xi_c^0 \rightarrow p K^-$	0	$\frac{\sqrt{6} s_c (-6R_c^{As} \bar{b} g_2' - 5R_c^{Au} (\bar{3}) \bar{b}' g_1' + 4R_c^{Au} (\bar{3}) \bar{b}' g_2' + 3R_c^{Au} (\bar{6}) \bar{b}' g_1' - 6R_c^{Au} (\bar{6}) \bar{b}' g_2')}{18}$
$\Xi_c^0 \rightarrow n K_{S/L}$	0	$\frac{\sqrt{3} s_c (-R_c^{As} \bar{b} g_1' + R_c^{Au} (\bar{6}) \bar{b}' g_1' - 2R_c^{Au} (\bar{6}) \bar{b}' g_2')}{3}$

TABLE XI. The legend is identical to that of Table IX but for DCS decays.

Channels	$\frac{\sqrt{2}}{G_F} \frac{1}{V_{cs}^* V_{ud} s_c^2} A^{\text{fac}}$	$\frac{f_P}{\sqrt{2} s_c^2} A^{\text{pole}}$
$\Lambda_c^+ \rightarrow n K^+$	$-\frac{\sqrt{6} C_+(A_1+A_2)}{12}$	$\frac{\sqrt{6} \bar{b}' (-R_c^{Au} (\bar{3}) (5g_1' - 4g_2') - 3R_c^{Au} (\bar{6}) (g_1' - 2g_2'))}{18}$
$\Xi_c^+ \rightarrow \Lambda^0 K^+$	$-\frac{C_+(A_1+A_2)}{12}$	$\frac{R_c^{As} \bar{b} (g_1' + g_2')}{3} - \frac{2R_c^{Au} (\bar{6}) \bar{b}' (g_1' - 2g_2')}{3}$
$\Xi_c^+ \rightarrow \Sigma^0 K^+$	$\frac{\sqrt{3} C_+(A_1+A_2)}{12}$	$\frac{\sqrt{3} R_c^{As} \bar{b} (g_1' - g_2')}{3}$
$\Xi_c^+ \rightarrow p \pi^0$	0	$\frac{\sqrt{3} (-6R_c^{As} \bar{b} g_2' - R_c^{Au} (\bar{3}) \bar{b}' (5g_1' - 4g_2') + 3R_c^{Au} (\bar{6}) \bar{b}' (g_1' - 2g_2'))}{18}$
$\Xi_c^+ \rightarrow p \eta$	0	$-\frac{R_c^{As} \bar{b} (2g_1' - g_2')}{3} + \frac{R_c^{Au} (\bar{3}) \bar{b}' (5g_1' - 4g_2')}{18} + \frac{R_c^{Au} (\bar{6}) \bar{b}' (g_1' - 2g_2')}{2}$
$\Xi_c^+ \rightarrow n \pi^+$	0	$\frac{\sqrt{6} (-6R_c^{As} \bar{b} g_2' - R_c^{Au} (\bar{3}) \bar{b}' (5g_1' - 4g_2') + 3R_c^{Au} (\bar{6}) \bar{b}' (g_1' - 2g_2'))}{18}$
$\Xi_c^0 \rightarrow \Sigma^- K^+$	$-\frac{\sqrt{6} C_+(A_1+A_2)}{12}$	$\frac{\sqrt{6} R_c^{As} \bar{b} (-g_1' + g_2')}{3}$
$\Xi_c^0 \rightarrow p \pi^-$	0	$\frac{\sqrt{6} (6R_c^{As} \bar{b} g_2' + R_c^{Au} (\bar{3}) \bar{b}' (5g_1' - 4g_2') - 3R_c^{Au} (\bar{6}) \bar{b}' (g_1' - 2g_2'))}{18}$
$\Xi_c^0 \rightarrow n \pi^0$	0	$\frac{\sqrt{3} (-6R_c^{As} \bar{b} g_2' - R_c^{Au} (\bar{3}) \bar{b}' (5g_1' - 4g_2') + 3R_c^{Au} (\bar{6}) \bar{b}' (g_1' - 2g_2'))}{18}$
$\Xi_c^0 \rightarrow n \eta$	0	$\frac{R_c^{As} \bar{b} (2g_1' - g_2')}{3} - \frac{R_c^{Au} (\bar{3}) \bar{b}' (5g_1' - 4g_2')}{18} - \frac{R_c^{Au} (\bar{6}) \bar{b}' (g_1' - 2g_2')}{2}$

TABLE XII. The parametrizations of A^{fac} and A^{pole} in the LP scenario for the decays of Ω_c^0 . The ones of B^{fac} and B^{pole} can be obtained by the substitutions in Eqs. (49) and (53).

Channels	$\frac{\sqrt{2}}{G_F} \frac{1}{V_{cs}^* V_{ud} f_P} A^{\text{fac}}$	$\frac{f_P}{\sqrt{2}} A^{\text{pole}}$
$\Omega_c \rightarrow \Xi^0 K_L$	$\frac{\sqrt{2} C_0(-A_1 s_c^2 + A_1 + A_2 s_c^2 - A_2)}{4}$	$\frac{\sqrt{2} (2R_c^{As} \bar{b} s_c^2 (2g_1' - g_2') - R_c^{Au} (\bar{3}) \bar{b}' (g_1' - 2g_2') - 3R_c^{Au} (\bar{6}) \bar{b}' g_1')}{6}$
$\Omega_c \rightarrow \Xi^0 K_S$	$\frac{\sqrt{2} C_0(-A_1 s_c^2 - A_1 + A_2 s_c^2 + A_2)}{4}$	$\frac{\sqrt{2} (2R_c^{As} \bar{b} s_c^2 (2g_1' - g_2') + R_c^{Au} (\bar{3}) \bar{b}' (g_1' - 2g_2') + 3R_c^{Au} (\bar{6}) \bar{b}' g_1')}{6}$
$\Omega_c \rightarrow \Lambda^0 K_{S/L}$	0	$\frac{\sqrt{3} s_c (-2R_c^{As} \bar{b} (2g_1' - g_2') + R_c^{Au} (\bar{3}) \bar{b}' (g_1' - 2g_2') + R_c^{Au} (\bar{6}) \bar{b}' g_1')}{6}$
$\Omega_c \rightarrow \Sigma^+ K^-$	0	$\frac{s_c (-6R_c^{As} \bar{b} g_2' + R_c^{Au} (\bar{3}) \bar{b}' (g_1' - 2g_2') - 3R_c^{Au} (\bar{6}) \bar{b}' g_1')}{3}$

(Table continued)

TABLE XII. (Continued)

Channels	$\frac{\sqrt{2}}{G_F V_{cs} V_{ud} f_P} A^{\text{fac}}$	$\frac{f_P}{\sqrt{2}} A^{\text{pole}}$
$\Omega_c \rightarrow \Sigma^0 K_{S/L}$	0	$\frac{s_c(6R_c^{As} \bar{b} g_2 - R_c^{Au} (\bar{3}) \bar{b}' (g_1 - 2g_2) + 3R_c^{Au} (\mathbf{6}) \bar{b}' g_1)}{6}$
$\Omega_c \rightarrow \Xi^0 \pi^0$	$\frac{\sqrt{2} s_c C_0 (A_1 - A_2)}{4}$	$\sqrt{2} R_c^{As} \bar{b} s_c (-g_1 + g_2)$
$\Omega_c \rightarrow \Xi^0 \eta$	$\frac{\sqrt{6} s_c C_0 (-A_1 + A_2)}{4}$	$\frac{\sqrt{6} s_c (R_c^{As} \bar{b} (g_1 + g_2) + 2R_c^{Au} (\mathbf{6}) \bar{b}' g_1)}{3}$
$\Omega_c \rightarrow \Xi^- \pi^+$	$\frac{s_c C_+ (A_1 - A_2)}{2}$	$2R_c^{As} \bar{b} s_c (g_1 - g_2)$
$\Omega_c \rightarrow \Lambda^0 \eta$	0	$\frac{2s_c^2 (R_c^{As} \bar{b} (g_1 - 2g_2) - 2R_c^{Au} (\mathbf{6}) \bar{b}' g_1)}{3}$
$\Omega_c \rightarrow \Sigma^+ \pi^-$	0	$\frac{2R_c^{As} \bar{b} s_c^2 (-g_1 + 2g_2)}{3}$
$\Omega_c \rightarrow \Sigma^0 \pi^0$	0	$\frac{2R_c^{As} \bar{b} s_c^2 (-g_1 + 2g_2)}{3}$
$\Omega_c \rightarrow \Sigma^- \pi^+$	0	$\frac{2R_c^{As} \bar{b} s_c^2 (-g_1 + 2g_2)}{3}$
$\Omega_c \rightarrow \Xi^- K^+$	$\frac{s_c^2 C_+ (A_1 - A_2)}{2}$	$\frac{2R_c^{As} \bar{b} s_c^2 (2g_1 - g_2)}{3}$
$\Omega_c \rightarrow p K^-$	0	$\frac{s_c^2 (-2R_c^{As} \bar{b} (g_1 + g_2) + R_c^{Au} (\bar{3}) \bar{b}' (g_1 - 2g_2) - 3R_c^{Au} (\mathbf{6}) \bar{b}' g_1)}{3}$
$\Omega_c \rightarrow n K_{S/L}$	0	$\frac{\sqrt{2} s_c^2 (-2R_c^{As} \bar{b} (g_1 + g_2) + R_c^{Au} (\bar{3}) \bar{b}' (g_1 - 2g_2) - 3R_c^{Au} (\mathbf{6}) \bar{b}' g_1)}{6}$

TABLE XIII. The parametrizations of A^{fac} and A^{pole} in the LP scenario for the CF decays of \mathbf{B}_{cc} . The ones of B^{fac} and B^{pole} can be obtained by the substitutions in Eqs. (49) and (53).

Channels	$\frac{\sqrt{2}}{G_F V_{cs} V_{ud} f_P} A^{\text{fac}}$	$\frac{f_P}{\sqrt{2}} A^{\text{pole}}$
$\Xi_{cc}^{++} \rightarrow \Sigma_c^{++} K_L$	$\frac{\sqrt{2} A_2 C_0 (1 - s_c^2)}{4}$	0
$\Xi_{cc}^{++} \rightarrow \Sigma_c^{++} K_S$	$-\frac{\sqrt{2} A_2 C_0 (s_c^2 + 1)}{4}$	0
$\Xi_{cc}^{++} \rightarrow \Xi_c^{++} \pi^+$	$\frac{\sqrt{2} A_2 C_+}{4}$	0
$\Xi_{cc}^{++} \rightarrow \Xi_c^{++} \pi^0$	$\frac{\sqrt{6} C_+ (-2A_1 + A_2)}{12}$	$\frac{2\sqrt{6} R_{cc}^{Au} \bar{b}' (-g_1 + g_2)}{3}$
$\Xi_{cc}^{++} \rightarrow \Sigma_c^{++} K^-$	0	$\frac{2R_{cc}^{As} (\bar{3}) \bar{b} (-g_1 + 2g_2)}{3}$
$\Xi_{cc}^{++} \rightarrow \Sigma_c^{++} K_L$	$\frac{A_2 C_0 (1 - s_c^2)}{4}$	$\frac{R_{cc}^{As} (\bar{3}) \bar{b} (-g_1 + 2g_2)}{3}$
$\Xi_{cc}^{++} \rightarrow \Sigma_c^{++} K_S$	$-\frac{A_2 C_0 (s_c^2 + 1)}{4}$	$\frac{R_{cc}^{As} (\bar{3}) \bar{b} (g_1 - 2g_2)}{3}$
$\Xi_{cc}^{++} \rightarrow \Xi_c^{++} \pi^0$	0	$\frac{R_{cc}^{As} (\bar{3}) \bar{b} (g_1 - 2g_2)}{3}$
$\Xi_{cc}^{++} \rightarrow \Xi_c^{++} \eta$	0	$\frac{\sqrt{3} R_{cc}^{As} (\bar{3}) \bar{b} (g_1 - 2g_2)}{3}$
$\Xi_{cc}^{++} \rightarrow \Xi_c^{++} \pi^+$	$\frac{\sqrt{2} A_2 C_+}{4}$	$\frac{\sqrt{2} R_{cc}^{As} (\bar{3}) \bar{b} (g_1 - 2g_2)}{3}$
$\Xi_{cc}^{++} \rightarrow \Omega_c K^+$	0	$\frac{2R_{cc}^{As} (\bar{3}) \bar{b} (g_1 - 2g_2)}{3}$
$\Xi_{cc}^{++} \rightarrow \Xi_c^0 \pi^+$	$\frac{\sqrt{6} C_+ (2A_1 - A_2)}{12}$	$\frac{\sqrt{6} R_{cc}^{As} (\bar{3}) \bar{b} (5g_1 - 4g_2)}{9}$
$\Xi_{cc}^{++} \rightarrow \Xi_c^0 \pi^0$	0	$\frac{\sqrt{3} (-R_{cc}^{As} (\bar{3}) \bar{b} (5g_1 - 4g_2) + 6R_{cc}^{Au} \bar{b}' (g_1 - g_2))}{9}$
$\Xi_{cc}^{++} \rightarrow \Xi_c^+ \eta$	0	$\frac{R_{cc}^{As} (\bar{3}) \bar{b} (5g_1 - 4g_2)}{9} - \frac{2R_{cc}^{Au} \bar{b}' (g_1 - g_2)}{3}$
$\Xi_{cc}^{++} \rightarrow \Lambda_c^+ K_L$	$\frac{\sqrt{3} C_0 (2A_1 s_c^2 - 2A_1 - A_2 s_c^2 + A_2)}{12}$	$\frac{\sqrt{3} (R_{cc}^{As} (\bar{3}) \bar{b} (5g_1 - 4g_2) - 6R_{cc}^{Au} \bar{b}' s_c^2 (g_1 - g_2))}{9}$
$\Xi_{cc}^{++} \rightarrow \Lambda_c^+ K_S$	$\frac{\sqrt{3} C_0 (2A_1 s_c^2 + 2A_1 - A_2 s_c^2 - A_2)}{12}$	$\frac{\sqrt{3} (-R_{cc}^{As} (\bar{3}) \bar{b} (5g_1 - 4g_2) - 6R_{cc}^{Au} \bar{b}' s_c^2 (g_1 - g_2))}{9}$
$\Omega_{cc}^+ \rightarrow \Xi_c^{++} K_L$	$\frac{A_2 C_0 (1 - s_c^2)}{4}$	$\frac{R_{cc}^{As} (\bar{3}) \bar{b} s_c^2 (g_1 - 2g_2)}{3}$
$\Omega_{cc}^+ \rightarrow \Xi_c^{++} K_S$	$-\frac{A_2 C_0 (s_c^2 + 1)}{4}$	$\frac{R_{cc}^{As} (\bar{3}) \bar{b} s_c^2 (g_1 - 2g_2)}{3}$
$\Omega_{cc}^+ \rightarrow \Omega_c \pi^+$	$\frac{A_2 C_+}{2}$	0
$\Omega_{cc}^+ \rightarrow \Xi_c^+ K_L$	$\frac{\sqrt{3} C_0 (-2A_1 s_c^2 + 2A_1 + A_2 s_c^2 - A_2)}{12}$	$\frac{\sqrt{3} (R_{cc}^{As} (\bar{3}) \bar{b} s_c^2 (5g_1 - 4g_2) - 6R_{cc}^{Au} \bar{b}' (g_1 - g_2))}{9}$
$\Omega_{cc}^+ \rightarrow \Xi_c^+ K_S$	$\frac{\sqrt{3} C_0 (-2A_1 s_c^2 - 2A_1 + A_2 s_c^2 + A_2)}{12}$	$\frac{\sqrt{3} (R_{cc}^{As} (\bar{3}) \bar{b} s_c^2 (5g_1 - 4g_2) + 6R_{cc}^{Au} \bar{b}' (g_1 - g_2))}{9}$

TABLE XIV. The legend is identical to that of Table XIII but for CS decays.

Channels	$\frac{\sqrt{2}}{G_F V_{cs}^* V_{ud} s_c f_P} A^{\text{fac}}$	$\frac{f_P}{\sqrt{2} s_c} A^{\text{pole}}$
$\Xi_{cc}^{++} \rightarrow \Sigma_c^{++} \pi^0$	$\frac{\sqrt{2} A_2 C_0}{4}$	0
$\Xi_{cc}^{++} \rightarrow \Sigma_c^{++} \eta$	$-\frac{\sqrt{6} A_2 C_0}{4}$	0
$\Xi_{cc}^{++} \rightarrow \Sigma_c^+ \pi^+$	$-\frac{\sqrt{2} A_2 C_+}{4}$	0
$\Xi_{cc}^{++} \rightarrow \Xi_c'^+ K^+$	$\frac{\sqrt{2} A_2 C_+}{4}$	0
$\Xi_{cc}^{++} \rightarrow \Xi_c^+ K^+$	$\frac{\sqrt{6} C_+ (-2A_1 + A_2)}{12}$	$\frac{2\sqrt{6} R_{cc}^{A_u} \bar{b}'(-g_1' + g_2')}{3}$
$\Xi_{cc}^{++} \rightarrow \Lambda_c^+ \pi^+$	$\frac{\sqrt{6} C_+ (-2A_1 + A_2)}{12}$	$\frac{2\sqrt{6} R_{cc}^{A_u} \bar{b}'(-g_1' + g_2')}{3}$
$\Xi_{cc}^+ \rightarrow \Sigma_c^{++} \pi^-$	0	$\frac{2R_{cc}^{A_s}(\bar{3})\bar{b}(g_1' - 2g_2')}{3}$
$\Xi_{cc}^+ \rightarrow \Sigma_c^+ \pi^0$	$\frac{A_2 C_0}{4}$	$\frac{2R_{cc}^{A_s}(\bar{3})\bar{b}(-g_1' + 2g_2')}{3}$
$\Xi_{cc}^+ \rightarrow \Sigma_c^+ \eta$	$-\frac{\sqrt{3} A_2 C_0}{4}$	0
$\Xi_{cc}^+ \rightarrow \Sigma_c^0 \pi^+$	$-\frac{A_2 C_+}{2}$	$\frac{2R_{cc}^{A_s}(\bar{3})\bar{b}(-g_1' + 2g_2')}{3}$
$\Xi_{cc}^+ \rightarrow \Xi_c'^+ K_{S/L}$	0	$\frac{R_{cc}^{A_s}(\bar{3})\bar{b}(g_1' - 2g_2')}{3}$
$\Xi_{cc}^+ \rightarrow \Xi_c'^0 K^+$	$\frac{\sqrt{2} A_2 C_+}{4}$	$\frac{\sqrt{2} R_{cc}^{A_s}(\bar{3})\bar{b}(-g_1' + 2g_2')}{3}$
$\Xi_{cc}^+ \rightarrow \Xi_c^0 K^+$	$\frac{\sqrt{6} C_+ (-2A_1 - A_2)}{12}$	$\frac{\sqrt{6} R_{cc}^{A_s}(\bar{3})\bar{b}(5g_1' - 4g_2')}{9}$
$\Xi_{cc}^+ \rightarrow \Xi_c^+ K_{S/L}$	0	$\frac{\sqrt{3}(R_{cc}^{A_s}(\bar{3})\bar{b}(5g_1' - 4g_2') - 6R_{cc}^{A_u} \bar{b}'(g_1' - g_2'))}{9}$
$\Xi_{cc}^+ \rightarrow \Lambda_c^+ \pi^0$	$\frac{\sqrt{3} C_0 (-2A_1 + A_2)}{12}$	$\frac{2\sqrt{3} R_{cc}^{A_u} \bar{b}'(g_1' - g_2')}{3}$
$\Xi_{cc}^+ \rightarrow \Lambda_c^+ \eta$	$\frac{C_0 (2A_1 - A_2)}{4}$	$-\frac{2R_{cc}^{A_s}(\bar{3})\bar{b}(5g_1' - 4g_2')}{9} - \frac{2R_{cc}^{A_u} \bar{b}'(g_1' - g_2')}{3}$
$\Omega_{cc}^+ \rightarrow \Sigma_c^{++} K^-$	0	$\frac{2R_{cc}^{A_s}(\bar{3})\bar{b}(-g_1' + 2g_2')}{3}$
$\Omega_{cc}^+ \rightarrow \Sigma_c^+ K_{S/L}$	0	$\frac{R_{cc}^{A_s}(\bar{3})\bar{b}(-g_1' + 2g_2')}{3}$
$\Omega_{cc}^+ \rightarrow \Xi_c'^+ \pi^0$	$\frac{A_2 C_0}{4}$	$\frac{R_{cc}^{A_s}(\bar{3})\bar{b}(g_1' - 2g_2')}{3}$
$\Omega_{cc}^+ \rightarrow \Xi_c'^+ \eta$	$-\frac{\sqrt{3} A_2 C_0}{4}$	$\frac{\sqrt{3} R_{cc}^{A_s}(\bar{3})\bar{b}(g_1' - 2g_2')}{3}$
$\Omega_{cc}^+ \rightarrow \Xi_c'^0 \pi^+$	$-\frac{\sqrt{2} A_2 C_+}{4}$	$\frac{\sqrt{2} R_{cc}^{A_s}(\bar{3})\bar{b}(g_1' - 2g_2')}{3}$
$\Omega_{cc}^+ \rightarrow \Omega_c K^+$	$\frac{A_2 C_+}{2}$	$\frac{2R_{cc}^{A_s}(\bar{3})\bar{b}(g_1' - 2g_2')}{3}$
$\Omega_{cc}^+ \rightarrow \Xi_c^0 \pi^+$	$\frac{\sqrt{6} C_+ (2A_1 - A_2)}{12}$	$\frac{\sqrt{6} R_{cc}^{A_s}(\bar{3})\bar{b}(5g_1' - 4g_2')}{9}$
$\Omega_{cc}^+ \rightarrow \Xi_c^+ \pi^0$	$\frac{\sqrt{3} C_0 (2A_1 - A_2)}{12}$	$\frac{\sqrt{3} R_{cc}^{A_s}(\bar{3})\bar{b}(-5g_1' + 4g_2')}{9}$
$\Omega_{cc}^+ \rightarrow \Xi_c^+ \eta$	$\frac{C_0 (-2A_1 + A_2)}{4}$	$\frac{R_{cc}^{A_s}(\bar{3})\bar{b}(5g_1' - 4g_2')}{9} + \frac{4R_{cc}^{A_u} \bar{b}'(g_1' - g_2')}{3}$
$\Omega_{cc}^+ \rightarrow \Lambda_c^+ K_{S/L}$	0	$\frac{\sqrt{3}(R_{cc}^{A_s}(\bar{3})\bar{b}(5g_1' - 4g_2') - 6R_{cc}^{A_u} \bar{b}'(g_1' - g_2'))}{9}$

TABLE XV. The legend is identical to that of Table XIII but for DCS decays.

Channels	$\frac{\sqrt{2}}{G_F V_{cs}^* V_{ud} s_c^2 f_P} A^{\text{fac}}$	$\frac{f_P}{\sqrt{2} s_c^2} A^{\text{pole}}$
$\Xi_{cc}^{++} \rightarrow \Sigma_c^+ K^+$	$-\frac{\sqrt{2} A_2 C_+}{4}$	0
$\Xi_{cc}^{++} \rightarrow \Lambda_c^+ K^+$	$\frac{\sqrt{6} C_+ (-2A_1 + A_2)}{12}$	$\frac{2\sqrt{6} R_{cc}^{A_u} \bar{b}'(-g_1' + g_2')}{3}$
$\Xi_{cc}^+ \rightarrow \Sigma_c^0 K^+$	$-\frac{A_2 C_+}{2}$	0
$\Omega_{cc}^+ \rightarrow \Sigma_c^{++} \pi^-$	0	$\frac{2R_{cc}^{A_s}(\bar{3})\bar{b}(g_1' - 2g_2')}{3}$
$\Omega_{cc}^+ \rightarrow \Sigma_c^+ \pi^0$	0	$\frac{2R_{cc}^{A_s}(\bar{3})\bar{b}(-g_1' + 2g_2')}{3}$
$\Omega_{cc}^+ \rightarrow \Sigma_c^0 \pi^+$	0	$\frac{2R_{cc}^{A_s}(\bar{3})\bar{b}(-g_1' + 2g_2')}{3}$
$\Omega_{cc}^+ \rightarrow \Xi_c'^0 K^+$	$-\frac{\sqrt{2} A_2 C_+}{4}$	$\frac{\sqrt{2} R_{cc}^{A_s}(\bar{3})\bar{b}(-g_1' + 2g_2')}{3}$
$\Omega_{cc}^+ \rightarrow \Xi_c^0 K^+$	$\frac{\sqrt{6} C_+ (2A_1 - A_2)}{12}$	$\frac{\sqrt{6} R_{cc}^{A_s}(\bar{3})\bar{b}(5g_1' - 4g_2')}{9}$
$\Omega_{cc}^+ \rightarrow \Lambda_c^+ \eta$	0	$-\frac{2R_{cc}^{A_s}(\bar{3})\bar{b}(5g_1' - 4g_2')}{9} + \frac{4R_{cc}^{A_u} \bar{b}'(g_1' - g_2')}{3}$

APPENDIX D: OPTIMIZATION AND EVALUATION WITH χ^2 ANALYSIS

The χ^2 function is defined as

$$\chi^2(\vec{x}) = \sum_{\text{exp}} \left(\frac{O_{\text{th}}(\vec{x}) - O_{\text{exp}}}{\sigma_{\text{exp}}} \right)^2, \quad (\text{D1})$$

where O_{th} denotes the theoretical value of an observable, contrasted with O_{exp} , the value observed in experiments, having a standard deviation of σ_{exp} . The vector \vec{x} aggregates all the free parameters in the theory.

The optimal solution \vec{x}_0 is one that minimizes the value of $\chi^2(\vec{x})$ across its entire domain, thereby satisfying $\chi^2(\vec{x}_0)$ as the minimal value. Given that \vec{x} is unbounded, the condition is established as follows:

$$\frac{\partial}{\partial \vec{x}} \chi^2 \Big|_{\vec{x}=\vec{x}_0} = 0, \quad \det |H(\vec{x}_0)| > 0, \quad (\text{D2})$$

Here, $H_{ij} := \partial_i \partial_j \chi^2$ represents the Hessian function. The covariance matrix is approximated excellently by the inverse of the Hessian function, represented as H^{-1} .

APPENDIX E: PREDICTIONS OF THE LP SCENARIO FOR $\mathbf{B}_c^A \rightarrow \mathbf{B}_n P$ AND $\mathbf{B}_{cc} \rightarrow \mathbf{B}_c^{A,S} P$

In the LP scenario, Tables XVI–XVIII present the numerical predictions for the \mathbf{B}_c^A decays. Likewise, Tables XIX and XX showcase the CS and DCS predictions for the \mathbf{B}_{cc} decays. These prognostications will serve as benchmarks for upcoming experimental validations and assessments.

TABLE XVI. Predictions of the LP scenario for the CF decays of $\mathbf{B}_c^A \rightarrow \mathbf{B}_n P$, where A and B are in units of $10^{-2} G_F \text{ GeV}^2$.

Channels	A^{fac}	A^{pole}	B^{fac}	B^{pole}	$\mathcal{B}(\%)$	α
$\Lambda_c^+ \rightarrow p K_L^0$	2.62	3.78	5.61	0.65	1.33(7)	-0.67(2)
$\Xi_c^+ \rightarrow \Sigma^+ K_S^0$	-2.75	0.34	-7.08	3.14	0.52(7)	-0.83(6)
$\Xi_c^+ \rightarrow \Sigma^+ K_L^0$	2.48	-0.74	6.37	-3.17	0.28(5)	-0.88(7)
$\Xi_c^0 \rightarrow \Sigma^0 K_L^0$	1.76	-0.91	4.51	-2.41	0.03(1)	-0.98(4)
$\Xi_c^0 \rightarrow \Xi^0 \pi^0$	0	5.15	0	4.62	0.73(9)	-0.51(6)
$\Xi_c^0 \rightarrow \Xi^0 \eta$	0	-3.12	0	-2.41	0.22(5)	-0.40(5)
$\Xi_c^0 \rightarrow \Lambda K_L^0$	1.07	3.64	2.55	1.89	0.57(4)	-0.60(3)

TABLE XVII. Predictions of the LP scenario for the CS decays of $\mathbf{B}_c^A \rightarrow \mathbf{B}_n P$, where A and B are in units of $10^{-2} G_F \text{ GeV}^2$.

Channels	A^{fac}	A^{pole}	B^{fac}	B^{pole}	$\mathcal{B}(10^{-4})$	α
$\Lambda_c^+ \rightarrow \Sigma^+ K_L^0$	0	0.99	0	0.75	2.84(35)	-0.41(5)
$\Xi_c^+ \rightarrow \Sigma^+ \pi^0$	0.50	1.19	1.29	0.26	24.21(2.59)	-0.58(3)
$\Xi_c^+ \rightarrow \Sigma^+ \eta$	-1.04	-0.28	-2.68	0.77	14.34(1.04)	-0.76(2)
$\Xi_c^+ \rightarrow \Sigma^0 \pi^+$	-0.59	-1.19	-1.51	-0.26	27.11(2.38)	-0.62(4)
$\Xi_c^+ \rightarrow \Xi^0 K^+$	-1.05	0.36	-3.07	1.11	5.34(1.92)	-0.97(2)
$\Xi_c^+ \rightarrow p K_{S/L}^0$	0	0.99	0	0.71	7.34(88)	-0.56(7)
$\Xi_c^+ \rightarrow \Lambda \pi^+$	0.36	-0.68	0.85	-0.91	0.80(38)	-0.14(31)
$\Xi_c^0 \rightarrow \Sigma^+ \pi^-$	0	-0.22	0	-0.22	0.14(19)	-0.63(23)
$\Xi_c^0 \rightarrow \Sigma^0 \pi^0$	0.36	0.62	0.91	-0.04	2.69(41)	-0.57(5)
$\Xi_c^0 \rightarrow \Sigma^0 \eta$	-0.74	-0.20	-1.90	0.55	2.40(17)	-0.76(2)
$\Xi_c^0 \rightarrow \Sigma^- \pi^+$	0.83	1.47	2.13	0.15	15.08(1.48)	-0.62(2)
$\Xi_c^0 \rightarrow \Xi^0 K_{S/L}^0$	0	-1.12	0	-0.92	2.97(38)	-0.44(4)
$\Xi_c^0 \rightarrow p K^-$	0	0.18	0	0.18	0.09(12)	-0.73(25)
$\Xi_c^0 \rightarrow n K_S^0$	0	-1.12	0	-0.84	3.14(40)	-0.58(5)
$\Xi_c^0 \rightarrow n K_L^0$	0	1.12	0	0.84	3.14(40)	-0.58(5)
$\Xi_c^0 \rightarrow \Lambda \pi^0$	0.22	-0.48	0.52	-0.64	0.18(9)	-0.35(25)
$\Xi_c^0 \rightarrow \Lambda \eta$	-0.45	-0.52	-1.07	0.02	2.45(29)	-0.66(4)

TABLE XVIII. Predictions of the LP scenario for the DCS decays of $\mathbf{B}_c^A \rightarrow \mathbf{B}_n P$, where A and B are in units of $10^{-2} G_F \text{ GeV}^2$.

Channels	A^{fac}	A^{pole}	B^{fac}	B^{pole}	$\mathcal{B}(10^{-5})$	α
$\Lambda_c^+ \rightarrow n K^+$	0.24	-0.04	0.52	-0.18	1.65(29)	-0.92(4)
$\Xi_c^+ \rightarrow \Sigma^0 K^+$	-0.16	-0.20	-0.42	-0.02	10.41(1.08)	-0.68(2)
$\Xi_c^+ \rightarrow p \pi^0$	0	0.04	0	0.05	0.13(14)	-0.93(22)
$\Xi_c^+ \rightarrow p \eta$	0	0.28	0	0.20	5.72(59)	-0.55(6)
$\Xi_c^+ \rightarrow n \pi^+$	0	0.05	0	0.08	0.27(29)	-0.93(22)
$\Xi_c^+ \rightarrow \Lambda K^+$	0.1	-0.18	0.23	-0.22	0.48(25)	0.1(27)
$\Xi_c^0 \rightarrow \Sigma^- K^+$	0.23	0.28	0.59	0.03	6.95(72)	-0.68(2)
$\Xi_c^0 \rightarrow p \pi^-$	0	-0.05	0	-0.08	0.09(10)	-0.93(22)
$\Xi_c^0 \rightarrow n \pi^0$	0	0.04	0	0.05	0.04(5)	-0.93(22)
$\Xi_c^0 \rightarrow n \eta$	0	-0.28	0	-0.20	1.90(20)	-0.55(6)

TABLE XIX. Predictions of the LP scenario for the CS decays of $\mathbf{B}_{cc} \rightarrow \mathbf{B}_c^{A,S}P$ with $\mathcal{C}_+ = 0.469$ and 1, where A and B are in units of $10^{-2}G_F \text{ GeV}^2$.

Channels	Results with $\mathcal{C}_+ = 0.469$						Results with $\mathcal{C}_+ = 1$	
	A^{fac}	A^{pole}	B^{fac}	B^{pole}	$\mathcal{B}(10^{-4})$	α	$\mathcal{B}(10^{-4})$	α
$\Xi_{cc}^{++} \rightarrow \Xi_c^+ K^+$	1.48	-0.23	2.10	-1.04	8.17(1.41)	-0.28(4)	46.12(1.41)	-0.39(4)
$\Xi_{cc}^{++} \rightarrow \Lambda_c^+ \pi^+$	1.39	-0.28	1.58	-1.25	7.47(1.46)	-0.14(7)	45.23(1.46)	-0.35(7)
$\Xi_{cc}^{++} \rightarrow \Sigma_c^{++} \pi^0$	0.48	0	3.22	0	5.45(55)	-0.97(0)	5.45(55)	-0.97(0)
$\Xi_{cc}^{++} \rightarrow \Sigma_c^{++} \eta$	-1.00	0	-6.69	0	18.06(18)	-0.99(0)	18.06(18)	-0.99(0)
$\Xi_{cc}^{++} \rightarrow \Sigma_c^+ \pi^+$	0.70	0	4.70	0	7.43(1.12)	-0.97(0)	34.03(1.12)	-0.97(0)
$\Xi_{cc}^{++} \rightarrow \Xi_c^+ K^+$	-0.77	0	-6.16	0	6.88(1.04)	-0.99(0)	31.51(1.04)	-0.99(0)
$\Xi_{cc}^{++} \rightarrow \Xi_c^0 K^+$	-1.47	-1.10	-2.10	0	4.89(48)	-0.27(1)	13.55(48)	-0.35(1)
$\Xi_{cc}^{++} \rightarrow \Xi_c^+ K_{S/L}$	0	-0.94	0	-0.74	0.66(8)	-0.26(3)	0.66(8)	-0.26(3)
$\Xi_{cc}^{++} \rightarrow \Lambda_c^+ \pi^0$	-0.67	0.20	-0.77	0.88	0.35(7)	-0.05(7)	0.35(7)	-0.05(7)
$\Xi_{cc}^{++} \rightarrow \Lambda_c^+ \eta$	1.40	0.80	1.59	-0.42	5.09(20)	-0.25(1)	5.09(20)	-0.25(1)
$\Xi_{cc}^{++} \rightarrow \Sigma_c^{++} \pi^-$	0	-0.52	0	0	0.21(6)	0(0)	0.21(6)	0(0)
$\Xi_{cc}^{++} \rightarrow \Sigma_c^+ \pi^0$	0.34	0.52	2.28	0	0.95(11)	-0.87(4)	0.95(11)	-0.87(4)
$\Xi_{cc}^{++} \rightarrow \Sigma_c^+ \eta$	-0.70	0	-4.73	0	1.27(0)	-0.99(0)	1.27(0)	-0.99(0)
$\Xi_{cc}^{++} \rightarrow \Sigma_c^0 \pi^+$	0.99	0.52	6.65	0	3.13(51)	-0.99(0)	11.55(51)	-1.00(0)
$\Xi_{cc}^{++} \rightarrow \Xi_c^+ K_{S/L}$	0	-0.21	0	0	0.03(1)	0(0)	0.03(1)	0(0)
$\Xi_{cc}^{++} \rightarrow \Xi_c^0 K^+$	-0.77	0.30	-6.16	0	0.71(10)	-0.81(3)	3.82(10)	-0.93(3)
$\Omega_{cc}^{++} \rightarrow \Xi_c^0 \pi^+$	-1.36	-1.32	-1.68	0	24.00(2.23)	-0.26(1)	60.65(2.23)	-0.34(1)
$\Omega_{cc}^{++} \rightarrow \Xi_c^+ \pi^0$	0.66	0.93	0.81	0	10.32(51)	-0.24(1)	10.32(51)	-0.24(1)
$\Omega_{cc}^{++} \rightarrow \Xi_c^+ \eta$	-1.37	-0.26	-1.69	0.85	11.75(75)	-0.24(2)	11.75(75)	-0.24(2)
$\Omega_{cc}^{++} \rightarrow \Lambda_c^+ K_{S/L}$	0	0.94	0	0.74	2.96(38)	-0.35(4)	2.96(38)	-0.35(4)
$\Omega_{cc}^{++} \rightarrow \Sigma_c^{++} K^-$	0	0.43	0	0	0.56(14)	0(0)	0.56(14)	0(0)
$\Omega_{cc}^{++} \rightarrow \Sigma_c^+ K_{S/L}$	0	-0.21	0	0	0.14(4)	0(0)	0.14(4)	0(0)
$\Omega_{cc}^{++} \rightarrow \Xi_c^+ \pi^0$	0.35	-0.26	2.38	0	1.09(6)	-0.58(9)	1.09(6)	-0.58(9)
$\Omega_{cc}^{++} \rightarrow \Xi_c^+ \eta$	-0.73	-0.37	-4.95	0	7.66(39)	-0.98(1)	7.66(39)	-0.98(1)
$\Omega_{cc}^{++} \rightarrow \Xi_c^0 \pi^+$	0.72	-0.36	4.92	0	3.10(45)	-0.67(5)	16.78(45)	-0.88(5)
$\Omega_{cc}^{++} \rightarrow \Omega_c^0 K^+$	-1.13	-0.43	-9.10	0	11.54(1.87)	-0.99(0)	44.67(1.87)	-1.00(0)

TABLE XX. Predictions of the LP scenario for the DCS decays of $\mathbf{B}_{cc} \rightarrow \mathbf{B}_c^{A,S}P$ with $\mathcal{C}_+ = 0.469$ and 1, where A and B are in units of $10^{-2}G_F \text{ GeV}^2$.

Channels	Results with $\mathcal{C}_+ = 0.469$						Results with $\mathcal{C}_+ = 1$	
	A^{fac}	A^{pole}	B^{fac}	B^{pole}	$\mathcal{B}(10^{-5})$	α	$\mathcal{B}(10^{-5})$	α
$\Xi_{cc}^{++} \rightarrow \Lambda_c^+ K^+$	0.38	-0.05	0.44	-0.24	6.18(1.03)	-0.25(4)	34.09(1.03)	-0.37(4)
$\Xi_{cc}^{++} \rightarrow \Sigma_c^+ K^+$	0.19	0	1.30	0	4.60(70)	-0.99(0)	21.07(70)	-0.99(0)
$\Xi_{cc}^{++} \rightarrow \Sigma_c^0 K^+$	0.27	0	1.84	0	1.29(20)	-0.99(0)	5.93(20)	-0.99(0)
$\Omega_{cc}^{++} \rightarrow \Xi_c^0 K^+$	-0.38	-0.25	-0.46	0	12.22(1.23)	-0.28(1)	34.98(1.23)	-0.35(1)
$\Omega_{cc}^{++} \rightarrow \Lambda_c^+ \eta$	0	0.25	0	0.20	2.05(25)	-0.35(4)	2.05(25)	-0.35(4)
$\Omega_{cc}^{++} \rightarrow \Sigma_c^{++} \pi^-$	0	-0.12	0	0	0.46(12)	0(0)	0.46(12)	0(0)
$\Omega_{cc}^{++} \rightarrow \Sigma_c^+ \pi^0$	0	0.12	0	0	0.46(12)	0(0)	0.46(12)	0(0)
$\Omega_{cc}^{++} \rightarrow \Sigma_c^0 \pi^+$	0	0.12	0	0	0.46(12)	0(0)	0.46(12)	0(0)
$\Omega_{cc}^{++} \rightarrow \Xi_c^0 K^+$	0.20	0.07	1.36	0	3.67(59)	-0.99(0)	14.36(59)	-1.00(0)

- [1] R. L. Workman *et al.* (Particle Data Group), Review of particle physics, *Prog. Theor. Exp. Phys.* **2022**, 083C01 (2022).
- [2] H. Y. Cheng, Charmed baryon physics circa 2021, *Chin. J. Phys.* **78**, 324 (2022).
- [3] S. Groote and J. G. Körner, Topological tensor invariants and the current algebra approach: Analysis of 196 non-leptonic two-body decays of single and double charm baryons—A review, *Eur. Phys. J. C* **82**, 297 (2022).
- [4] M. Ablikim *et al.* (BESIII Collaboration), Precision measurement of the integrated luminosity of the data taken by BESIII at center of mass energies between 3.810 GeV and 4.600 GeV, *Chin. Phys. C* **39**, 093001 (2015).
- [5] M. Ablikim *et al.* (BESIII Collaboration), Measurements of absolute hadronic branching fractions of Λ_c^+ baryon, *Phys. Rev. Lett.* **116**, 052001 (2016); Measurements of absolute branching fractions for $\Lambda_c^+ \rightarrow \Xi^0 K^+$ and $\Xi(1530)^0 K^+$, *Phys. Lett. B* **783**, 200 (2018); Evidence for the decays of $\Lambda_c^+ \rightarrow \Sigma^+ \eta$ and $\Sigma^+ \eta'$, *Chin. Phys. C* **43**, 083002 (2019); Measurement of branching fractions of singly Cabibbo-suppressed decays $\Lambda_c^+ \rightarrow \Sigma^0 K^+$ and $\Sigma^+ K_S^0$, *Phys. Rev. D* **106**, 052003 (2022).
- [6] M. Ablikim *et al.* (BESIII Collaboration), Measurement of branching fractions of singly Cabibbo-suppressed decays $\Lambda_c^+ \rightarrow \Sigma^0 K^+$ and $\Sigma^+ K_S^0$, *Phys. Rev. D* **106**, 052003 (2022).
- [7] M. Ablikim *et al.* (BESIII Collaboration), Measurement of the branching fraction of the singly Cabibbo-suppressed decay $\Lambda_c^+ \rightarrow \Lambda K^+$, *Phys. Rev. D* **106**, L111101 (2022); Measurement of the branching fractions of the singly Cabibbo-suppressed decays $\Lambda_c^+ \rightarrow p \eta$ and $\Lambda_c^+ \rightarrow p \omega$, *J. High Energy Phys.* **11** (2023) 137.
- [8] M. Ablikim *et al.* (BESIII Collaboration), Observation of the singly Cabibbo suppressed decay $\Lambda_c^+ \rightarrow n \pi^+$, *Phys. Rev. Lett.* **128**, 142001 (2022).
- [9] R. Chistov *et al.* (Belle Collaboration), First observation of Cabibbo-suppressed Ξ_c^0 decays, *Phys. Rev. D* **88**, 071103 (2013).
- [10] S. B. Yang *et al.* (Belle Collaboration), First observation of doubly Cabibbo-suppressed decay of a charmed baryon: $\Lambda_c^+ \rightarrow p K^+ \pi^-$, *Phys. Rev. Lett.* **117**, 011801 (2016); Y. B. Li *et al.* (Belle Collaboration), First measurements of absolute branching fractions of the Ξ_c^+ baryon at Belle, *Phys. Rev. D* **100**, 031101 (2019); S. Jia *et al.* (Belle Collaboration), Measurements of branching fractions and asymmetry parameters of $\Xi_c^0 \rightarrow \Lambda \bar{K}^{*0}$, $\Xi_c^0 \rightarrow \Sigma^0 \bar{K}^{*0}$, and $\Xi_c^0 \rightarrow \Sigma^+ K^{*-}$ decays at Belle, *J. High Energy Phys.* **06** (2021) 160; S. X. Li *et al.* (Belle Collaboration), First measurement of the $\Lambda_c^+ \rightarrow p \eta'$ decay, *J. High Energy Phys.* **03** (2022) 090; Measurement of branching fractions of $\Lambda_c^+ \rightarrow p K_S^0 K_S^0$ and $\Lambda_c^+ \rightarrow p K_S^0 \eta$ at Belle, *Phys. Rev. D* **107**, 032004 (2023).
- [11] Y. Li *et al.* (Belle Collaboration), Measurements of the branching fractions of $\Xi_c^0 \rightarrow \Lambda K_S^0$, $\Xi_c^0 \rightarrow \Sigma^0 K_S^0$, and $\Xi_c^0 \rightarrow \Sigma^+ K^-$ decays at Belle, *Phys. Rev. D* **105**, L011102 (2022).
- [12] L. K. Li *et al.* (Belle Collaboration), Search for CP violation and measurement of branching fractions and decay asymmetry parameters for $\Lambda_c^+ \rightarrow \Lambda h^+$ and $\Lambda_c^+ \rightarrow \Sigma^0 h^+$ ($h = K, \pi$), *Sci. Bull.* **68**, 583 (2023); Measurements of branching fractions of $\Lambda_c^+ \rightarrow \Sigma^+ \eta$ and $\Lambda_c^+ \rightarrow \Sigma^+ \eta'$ and asymmetry parameters of $\Lambda_c^+ \rightarrow \Sigma^+ \pi^0$, $\Lambda_c^+ \rightarrow \Sigma^+ \eta$, and $\Lambda_c^+ \rightarrow \Sigma^+ \eta'$, *Phys. Rev. D* **107**, 032003 (2023).
- [13] Y. B. Li *et al.* (Belle Collaboration), First measurements of absolute branching fractions of the Ξ_c^0 baryon at Belle, *Phys. Rev. Lett.* **122**, 082001 (2019).
- [14] Y. B. Li *et al.* (Belle Collaboration), Measurements of the branching fractions of the semileptonic decays $\Xi_c^0 \rightarrow \Xi^- \ell^+ \nu_\ell$ and the asymmetry parameter of $\Xi_c^0 \rightarrow \Xi^- \pi^+$, *Phys. Rev. Lett.* **127**, 121803 (2021).
- [15] X. G. He, F. Huang, W. Wang, and Z. P. Xing, SU(3) symmetry and its breaking effects in semileptonic heavy baryon decays, *Phys. Lett. B* **823**, 136765 (2021); C. Q. Geng, X. N. Jin, and C. W. Liu, Resolving puzzle in $\Xi_c^0 \rightarrow \Xi^- e^+ \nu_e$ with $\Xi_c - \Xi_c'$ mixing spectrum within the quark model, *Phys. Lett. B* **838**, 137736 (2023).
- [16] R. Aaij *et al.* (LHCb Collaboration), Observation of excited Ω_c^0 baryons in $\Omega_b^- \rightarrow \Xi_c^+ K^- \pi^-$ decays, *Phys. Rev. D* **104**, L091102 (2021).
- [17] R. Aaij *et al.* (LHCb Collaboration), Observation of the doubly charmed baryon Ξ_{cc}^{++} , *Phys. Rev. Lett.* **119**, 112001 (2017); Precision measurement of the Ξ_{cc}^{++} mass, *J. High Energy Phys.* **02** (2020) 049.
- [18] F. J. Abudinen *et al.* (Belle-II Collaboration), Measurement of the Ω_c^0 lifetime at Belle II, *Phys. Rev. D* **107**, L031103 (2023); Measurement of the Λ_c^+ lifetime, *Phys. Rev. Lett.* **130**, 071802 (2023); , Measurement of charm baryon lifetimes at Belle II, *Few-Body Syst.* **64**, 64 (2023).
- [19] R. Aaij *et al.* (LHCb Collaboration), Measurement of the Ω_c^0 baryon lifetime, *Phys. Rev. Lett.* **121**, 092003 (2018); Precision measurement of the Λ_c^+ , Ξ_c^+ and Ξ_c^0 baryon lifetimes, *Phys. Rev. D* **100**, 032001 (2019).
- [20] S. Eidelman *et al.* (Particle Data Group), Review of particle physics, *Phys. Lett. B* **592**, 1 (2004).
- [21] H. Y. Cheng, Phenomenological study of heavy hadron lifetimes, *J. High Energy Phys.* **11** (2018) 014; The strangest lifetime: A bizarre story of $\tau(\Omega_c^0)$, *Sci. Bull.* **67**, 445 (2022).
- [22] J. Gratx, B. Melić, and I. Nišandžić, Lifetimes of singly charmed hadrons, *J. High Energy Phys.* **07** (2022) 058; H. Y. Cheng and C. W. Liu, Study of singly heavy baryon lifetimes, *J. High Energy Phys.* **07** (2023) 114.
- [23] L. Dulibić, J. Gratx, B. Melić, and I. Nišandžić, Revisiting lifetimes of doubly charmed baryons, *J. High Energy Phys.* **07** (2023) 061.
- [24] A. Lenz and T. Rauh, D-meson lifetimes within the heavy quark expansion, *Phys. Rev. D* **88**, 034004 (2013); D. King, A. Lenz, M. L. Piscopo, T. Rauh, A. V. Rusov, and C. Vlahos, Revisiting inclusive decay widths of charmed mesons, *J. High Energy Phys.* **08** (2022) 241.
- [25] B. Guberina, S. Nussinov, R. D. Peccei, and R. Ruckl, D meson lifetimes and decays, *Phys. Lett.* **89B**, 111 (1979); N. Bilic, B. Guberina, and J. Trampetic, Pauli interference effect in D + lifetime, *Nucl. Phys.* **B248**, 261 (1984); B. Guberina, R. Ruckl, and J. Trampetic, Charmed baryon lifetime differences, *Z. Phys. C* **33**, 297 (1986); M. Neubert and C. T. Sachrajda, Spectator effects in inclusive decays of beauty hadrons, *Nucl. Phys.* **B483**, 339 (1997).
- [26] H. Y. Cheng and B. Tseng, Nonleptonic weak decays of charmed baryons, *Phys. Rev. D* **46**, 1042 (1992); **55**, 1697(E) (1997).

- [27] Q. P. Xu and A. N. Kamal, Cabibbo favored nonleptonic decays of charmed baryons, *Phys. Rev. D* **46**, 270 (1992).
- [28] J. G. Korner and M. Kramer, Exclusive nonleptonic charm baryon decays, *Z. Phys. C* **55**, 659 (1992).
- [29] H. Y. Cheng and B. Tseng, Cabibbo allowed nonleptonic weak decays of charmed baryons, *Phys. Rev. D* **48**, 4188 (1993).
- [30] T. Uppal, R. C. Verma, and M. P. Khanna, Constituent quark model analysis of weak mesonic decays of charm baryons, *Phys. Rev. D* **49**, 3417 (1994).
- [31] M. A. Ivanov, J. G. Korner, V. E. Lyubovitskij, and A. G. Rusetsky, Exclusive nonleptonic decays of bottom and charm baryons in a relativistic three quark model: Evaluation of nonfactorizing diagrams, *Phys. Rev. D* **57**, 5632 (1998).
- [32] K. K. Sharma and R. C. Verma, A study of weak mesonic decays of Λ_c and Ξ_c baryons on the basis of HQET results, *Eur. Phys. J. C* **7**, 217 (1999).
- [33] H. Y. Cheng, X. W. Kang, and F. Xu, Singly Cabibbo-suppressed hadronic decays of Λ_c^+ , *Phys. Rev. D* **97**, 074028 (2018).
- [34] T. Gutsche, M. A. Ivanov, J. G. Körner, and V. E. Lyubovitskij, Nonleptonic two-body decays of single heavy baryons Λ_Q , Ξ_Q , and Ω_Q ($Q = b, c$) induced by W emission in the covariant confined quark model, *Phys. Rev. D* **98**, 074011 (2018).
- [35] S. Hu, G. Meng, and F. Xu, Hadronic weak decays of the charmed baryon Ω_c^0 , *Phys. Rev. D* **101**, 094033 (2020).
- [36] G. Meng, S. M. Y. Wong, and F. Xu, Doubly Cabibbo-suppressed decays of antitriplet charmed baryons, *J. High Energy Phys.* **11** (2020) 126.
- [37] P. Y. Niu, J. M. Richard, Q. Wang, and Q. Zhao, Hadronic weak decays of Λ_c in the quark model, *Phys. Rev. D* **102**, 073005 (2020).
- [38] J. Zou, F. Xu, G. Meng, and H. Y. Cheng, Two-body hadronic weak decays of antitriplet charmed baryons, *Phys. Rev. D* **101**, 014011 (2020).
- [39] F. Xu, Q. Wen, and H. Zhong, $K_S^0 - K_L^0$ asymmetries in weak decays of charmed baryons, *Lett. High Energy Phys.* **2021**, 218 (2021).
- [40] S. Zeng, F. Xu, P. Y. Niu, and H. Y. Cheng, Doubly charmed baryon decays $\Xi_{cc}^{++} \rightarrow \Xi_c^{(+) +} \pi^+$ in the quark model, *Phys. Rev. D* **107**, 034009 (2023).
- [41] M. J. Savage and R. P. Springer, SU(3) predictions for charmed baryon decays, *Phys. Rev. D* **42**, 1527 (1990).
- [42] L. L. Chau, H. Y. Cheng, and B. Tseng, Analysis of two-body decays of charmed baryons using the quark diagram scheme, *Phys. Rev. D* **54**, 2132 (1996).
- [43] K. K. Sharma and R. C. Verma, SU(3) flavor analysis of two-body weak decays of charmed baryons, *Phys. Rev. D* **55**, 7067 (1997).
- [44] C. D. Lü, W. Wang, and F. S. Yu, Test flavor SU(3) symmetry in exclusive Λ_c decays, *Phys. Rev. D* **93**, 056008 (2016).
- [45] C. Q. Geng, Y. K. Hsiao, C. W. Liu, and T. H. Tsai, Charmed baryon weak decays with SU(3) flavor symmetry, *J. High Energy Phys.* **11** (2017) 147.
- [46] C. Q. Geng, Y. K. Hsiao, C. W. Liu, and T. H. Tsai, Antitriplet charmed baryon decays with SU(3) flavor symmetry, *Phys. Rev. D* **97**, 073006 (2018).
- [47] C. Q. Geng, Y. K. Hsiao, C. W. Liu, and T. H. Tsai, SU(3) symmetry breaking in charmed baryon decays, *Eur. Phys. J. C* **78**, 593 (2018).
- [48] C. Q. Geng, Y. K. Hsiao, C. W. Liu, and T. H. Tsai, Three-body charmed baryon decays with SU(3) flavor symmetry, *Phys. Rev. D* **99**, 073003 (2019).
- [49] C. Q. Geng, C. W. Liu, and T. H. Tsai, Singly Cabibbo suppressed decays of Λ_c^+ with SU(3) flavor symmetry, *Phys. Lett. B* **790**, 225 (2019).
- [50] C. Q. Geng, C. W. Liu, and T. H. Tsai, Asymmetries of antitriplet charmed baryon decays, *Phys. Lett. B* **794**, 19 (2019).
- [51] D. Wang, Sum rules for CP asymmetries of charmed baryon decays in the $SU(3)_F$ limit, *Eur. Phys. J. C* **79**, 429 (2019).
- [52] C. Q. Geng, C. W. Liu, T. H. Tsai, and Y. Yu, Charmed baryon weak decays with decuplet baryon and SU(3) flavor symmetry, *Phys. Rev. D* **99**, 114022 (2019).
- [53] C. P. Jia, D. Wang, and F. S. Yu, Charmed baryon decays in $SU(3)_F$ symmetry, *Nucl. Phys.* **B956**, 115048 (2020).
- [54] J. Y. Cen, C. Q. Geng, C. W. Liu, and T. H. Tsai, Up-down asymmetries of charmed baryon three-body decays, *Eur. Phys. J. C* **79**, 946 (2019).
- [55] C. Q. Geng, C. W. Liu, and T. H. Tsai, Charmed baryon weak decays with vector mesons, *Phys. Rev. D* **101**, 053002 (2020).
- [56] X. G. He, Y. J. Shi, and W. Wang, Unification of flavor SU(3) analyses of heavy hadron weak decays, *Eur. Phys. J. C* **80**, 359 (2020).
- [57] Y. K. Hsiao, Y. L. Wang, and H. J. Zhao, Equivalent $SU(3)_f$ approaches for two-body anti-triplet charmed baryon decays, *J. High Energy Phys.* **09** (2022) 035.
- [58] F. Huang, Z. P. Xing, and X. G. He, A global analysis of charmless two body hadronic decays for anti-triplet charmed baryons, *J. High Energy Phys.* **03** (2022) 143; **09** (2022) 87(E).
- [59] H. Zhong, F. Xu, Q. Wen, and Y. Gu, Weak decays of antitriplet charmed baryons from the perspective of flavor symmetry, *J. High Energy Phys.* **02** (2023) 235.
- [60] D. Wang, Generation of SU(3) sum rule for charmed baryon decay, *J. High Energy Phys.* **12** (2022) 003.
- [61] Z. P. Xing, X. G. He, F. Huang, and C. Yang, A global analysis for determined and undetermined hadronic two body weak decays of anti-triplet charmed baryons, *Phys. Rev. D* **108**, 053004 (2023).
- [62] J. G. Körner, Octet behaviour of single-particle matrix elements $\langle B'|H(W)|B\rangle$ and $\langle M'|H(W)|M\rangle$ using a weak current current quark Hamiltonian, *Nucl. Phys.* **B25**, 282 (1971); J. C. Pati and C. H. Woo, Delta $I = 1/2$ rule with fermion quarks, *Phys. Rev. D* **3**, 2920 (1971).
- [63] G. Buchalla, A. J. Buras, and M. E. Lautenbacher, Weak decays beyond leading logarithms, *Rev. Mod. Phys.* **68**, 1125 (1996).
- [64] H. Y. Cheng and C. K. Chua, On the smallness of tree-dominated charmless two-body baryonic B decay rates, *Phys. Rev. D* **91**, 036003 (2015).
- [65] S. Meinel, $\Lambda_c \rightarrow \Lambda l^+ \nu_l$ form factors and decay rates from lattice QCD with physical quark masses, *Phys. Rev. Lett.* **118**, 082001 (2017).
- [66] S. Meinel, $\Lambda_c \rightarrow N$ form factors from lattice QCD and phenomenology of $\Lambda_c \rightarrow n \ell^+ \nu_\ell$ and $\Lambda_c \rightarrow p \mu^+ \mu^-$ decays, *Phys. Rev. D* **97**, 034511 (2018).

- [67] C. Q. Geng, X. N. Jin, and C. W. Liu, Anatomy of $\Lambda_c +$ semileptonic decays, *Phys. Rev. D* **107**, 033008 (2023).
- [68] H. Y. Cheng, Contributions of parity violating baryon matrix elements to nonleptonic charmed baryon decays, *Z. Phys. C* **29**, 453 (1985).
- [69] T. M. Yan, H. Y. Cheng, C. Y. Cheung, G. L. Lin, Y. C. Lin, and H. L. Yu, Heavy quark symmetry and chiral dynamics, *Phys. Rev. D* **46**, 1148 (1992); **55**, 5851(E) (1997).
- [70] G. L. Yu, Z. Y. Li, Z. G. Wang, J. Lu, and M. Yan, Systematic analysis of doubly charmed baryons Ξ_{cc} and Ω_{cc} , *Eur. Phys. J. A* **59**, 126 (2023).
- [71] C. W. Liu and C. Q. Geng, Center of mass motion in bag model, *Chin. Phys. C* **47**, 014104 (2023). Details pertaining to the Ω_c^0 form factors and semileptonic decays are expected to appear on arXiv in the next few months.
- [72] R. Aaij *et al.* (LHCb Collaboration), Observation of the doubly charmed baryon decay $\Xi_{cc}^{++} \rightarrow \Xi_c'^+ \pi^+$, *J. High Energy Phys.* **05** (2022) 038.
- [73] H. Y. Cheng, G. Meng, F. Xu, and J. Zou, Two-body weak decays of doubly charmed baryons, *Phys. Rev. D* **101**, 034034 (2020).
- [74] C. W. Liu and C. Q. Geng, Nonleptonic decays of $\Xi_{cc} \rightarrow \Xi_c \pi$ with $\Xi_c - \Xi_c'$ mixing, *Phys. Rev. D* **107**, 013006 (2023).
- [75] A. Chodos, R. L. Jaffe, K. Johnson, C. B. Thorn, and V. F. Weisskopf, A new extended model of hadrons, *Phys. Rev. D* **9**, 3471 (1974).
- [76] Y. Chen, W.-F. Chiu, M. Gong, Z. Liu, and Y. Ma (χ QCD Collaboration), Charmed and ϕ meson decay constants from $2 + 1$ -flavor lattice QCD, *Chin. Phys. C* **45**, 023109 (2021).